Physica D 239 (2010) 1542–1559

Contents lists available at ScienceDirect

Physica D

journal homepage: www.elsevier.com/locate/physd

A moving boundary model motivated by electric breakdown: II. Initial value problem

C.-Y. Kao [a], F. Brau [b,c], U. Ebert [b,d,*], L. Schäfer [e], S. Tanveer [a]

[a] Department of Mathematics, Ohio State University, OH 43210, USA

[b] Centrum Wiskunde & Informatica (CWI), P.O. Box 94079, NL-1090GB Amsterdam, The Netherlands

[c] Groupe de Physique Nucleaire Théorique, Université de Mons-Hainaut, Académie Universitaire Wallonie-Bruxelles, Place du Parc 20, B-7000 Mons, Belgium

[d] Department of Physics, Eindhoven University of Technology, P.O. Box 513, NL-5600MB Eindhoven, The Netherlands

[e] Fachbereich Physik, Universität Duisburg-Essen, Lotharstrasse 1, D-47048 Duisburg, Germany

ARTICLE INFO

Article history:
Received 17 August 2009
Received in revised form
22 March 2010
Accepted 29 March 2010
Available online 13 April 2010
Communicated by B. Sandstede

Keywords:
Moving boundary
Kinetic undercooling regularization
Initial value problem
Laplacian instability
Electric breakdown

ABSTRACT

An interfacial approximation of the streamer stage in the evolution of sparks and lightning can be formulated as a Laplacian growth model regularized by a 'kinetic undercooling' boundary condition. Using this model we study both the linearized and the full nonlinear evolution of small perturbations of a uniformly translating circle. Within the linear approximation analytical and numerical results show that perturbations are advected to the back of the circle, where they decay. An initially analytic interface stays analytic for all finite times, but singularities from outside the physical region approach the interface for $t \to \infty$, which results in some anomalous relaxation at the back of the circle. For the nonlinear evolution numerical results indicate that the circle is the asymptotic attractor for small perturbations, but larger perturbations may lead to branching. We also present results for more general initial shapes, which demonstrate that regularization by kinetic undercooling cannot guarantee smooth interfaces globally in time.

1. Introduction

Propagating fronts in Laplacian growth occur naturally in quite a number of physical problems including viscous fingering [1–5], electro-chemical growth, dendritic crystal growth for small undercooling [6–8], and void migration in a conductor [9–11]. More recently, it has been shown that this class of problems includes the 'streamer' stage of electric breakdown [12–19], which will be described below. A central issue in these problems is the stability of curved fronts. In a limiting case, most of these models reduce to the classic Saffman–Taylor problem [1], which is known to be ill-posed [20,21]. Numerical as well as formal asymptotic results [4,8,5,22] suggest that one branch of steadily propagating finger or bubble solutions in a Hele–Shaw cell is stabilized by surface tension regularization, though only recently some mathematically rigorous results [23,24] are available to justify nonlinear stability to small disturbances in the special case of a nearly circular bubble. Besides surface tension, other regularizations [9–11,25] have also been analyzed. In the present paper we study both the linear and the nonlinear initial value problem for one such regularization, in particular, the stability of a steadily propagating circular shape. This regularization is called kinetic undercooling in the crystal growth context,[1] but has a different physical interpretation for streamers.

During the streamer stage of electric breakdown the discharge paves its way through a nonconducting medium, leaving behind a weakly ionized conducting channel. The basic growth mechanism is impact ionization due to electrons strongly accelerated in the local electric field. In a sufficiently strong field, a thin space charge layer forms around the head of the streamer. This layer screens the field in the inner ionized region to a very low level, and the growth of the streamer is driven by the electrons moving and multiplying in the strong self-enhanced field ahead of the curved ionization front.

For sufficiently strong external fields, the thickness ℓ of the electron layer is small compared to the radius R of the streamer

* Corresponding author at: Centrum Wiskunde & Informatica (CWI), P.O. Box 94079, NL-1090GB Amsterdam, The Netherlands.
E-mail address: ebert@cwi.nl (U. Ebert).

[1] In crystal growth, kinetic undercooling is likely to be the more important regularization compared to the Gibbs–Thompson effect for large undercooling where the Laplacian growth model becomes questionable. This happens when the time scale over which the interface evolves becomes comparable to the time scale of heat diffusion.

0167-2789/$ – see front matter © 2010 Elsevier B.V. All rights reserved.
doi:10.1016/j.physd.2010.03.011

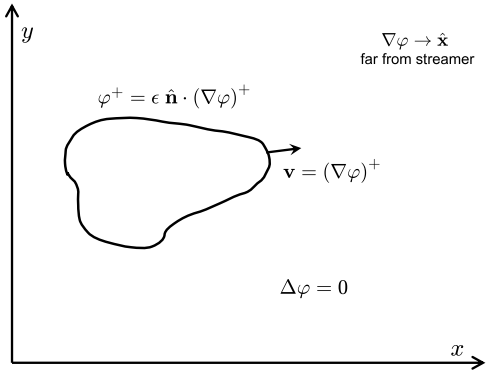

Fig. 1. Illustration of the model problem in terms of the Laplace field φ.

head. Therefore Lozansky and Firsov suggested (mainly in the Russian literature, but also in [26]) that this layer can be modeled as an interface separating the ionized from the non-ionized region. Probably, the idea is even older, since a similar concept was already proposed by Sämmer in the German literature in 1933 [27]. However, a deeper study of the implications of this concept started only later [12–14,28–30] where the problem is placed in the context of other Laplacian moving boundary problems. The validity of the moving boundary approximation for negative streamers is discussed in [15] for simple gases like pure nitrogen or argon, and in [31] for air. The dimensional analysis and the proposed regularization mechanism of the moving boundary problem for negative streamer ionization fronts are discussed in detail in our previous papers [16–19].

In dimensionless form, the model is defined as follows, see Fig. 1 for an illustration. The normal velocity v_n of the interface is given by the drift velocity $\mathbf{v}$ of the electrons, which is proportional to the local electrostatic field $\mathbf{E} = -\nabla\varphi$. In appropriate units it takes the dimensionless form:

$$v_n = -\hat{\mathbf{n}} \cdot \mathbf{E}^+, \tag{1}$$

where the superscript $^+$ denotes the limiting value as the interface is approached from the exterior (the non-ionized region) and $\hat{\mathbf{n}}$ is the outward normal on the interface. Outside the streamer the electric potential φ obeys the Laplace equation:

$$\Delta\varphi = 0. \tag{2}$$

An analytical and numerical analysis of the underlying physical model formulated in terms of partial differential equations for the charged densities and the field suggests the interfacial condition

$$\varphi^+ = \epsilon\hat{\mathbf{n}} \cdot (\nabla\varphi)^+, \tag{3}$$

where

$$\epsilon = \frac{\ell}{R}. \tag{4}$$

Far from the streamer, the electric field tends to a constant[2]

$$\mathbf{E} = -\nabla\varphi \to -\hat{\mathbf{x}} + o(1/|\mathbf{x}|), \tag{5}$$

where $\hat{\mathbf{x}}$ is the unit vector in the x-direction. Eqs. (1)–(5) define our model.

In two dimensions, a simple solution to the free boundary problem posed by this model takes the form of a uniformly translating circle. Our previous work in [17–19] and the present paper are primarily concerned with the linear and nonlinear stability of this solution to small perturbations. It is to be noted that the circular shape differs from an actual streamer shape. However, the front half of a circle roughly resembles the shape of the front part of a streamer. Since growth of disturbances is found to be most pronounced in this advancing part of the interface, we expect stability features found here to be qualitatively relevant for an actual streamer and more generally for curved fronts.

In the special case $\epsilon = 1$, the linearized evolution of small perturbations can be determined exactly in our model [17,18]. The case of general $\epsilon > 0$ is treated in part I [19] of this series of papers and in the present manuscript. In [19], we discussed the spectrum of the linear operator which results from the linear stability analysis of the circular solution. Restricting ourselves to an appropriate space of analytic perturbations we found a pure point spectrum. Asymptotically in time, except for the trivial translation mode, all eigenmodes were found to decay exponentially in time. These eigenmodes are singular at the back of the bubble; nonetheless, as evidenced in the present paper, this singularity is not reflected by the actual linear evolution near the bubble back. The usual asymptotic form of the solution for large time: $\sum_\lambda e^{\lambda t}\beta_\lambda$, where β_λ is the eigenfunction corresponding to the eigenvalue λ, fails in a neighborhood of the rear of the bubble, though it holds elsewhere.

In the present paper, we consider the initial value problem. For the linearized evolution, analytical results are obtained in the limit of strongly localized disturbances of the circle. Also the large time behavior of general perturbations can be studied analytically. Numerical calculations confirm these results. Together with the eigenvalue analysis of the first paper [19], clear evidence of linear stability is presented. The full nonlinear evolution of a perturbed interface is calculated numerically. Our results suggest that, similar to linear evolution, small enough perturbations of a circular bubble grow in the front part of the bubble, but eventually decay as interfacial distortions advect to the bubble rear. Nonetheless, when ϵ is small but nonzero, the large transients in the linear regime make nonlinearity important even when the initial perturbation is exponentially small in ϵ. Furthermore, when the perturbations are larger, the circle is no longer an attractor of the dynamics and the propagating structure branches. For general initial shapes, we give some numerical evidence that the undercooling regularization condition cannot guarantee a smooth interface globally in time. For some initial conditions, the interface tends to develop a sharp corner in the back. Other initial conditions lead to the separation of the moving body into two parts.

This paper is organized as follows. In Section 2 we present equations derived earlier in a conformal map setting. Section 3 is devoted to the linear evolution of perturbations of the circle. Section 3.1 recalls previous results, and in Section 3.2 we present rigorous results on the growth of a strongly localized perturbation. We continue the discussion of localized perturbations in Section 3.3 and explain at an intuitive level how strongly localized perturbations are generically advected to the rear of the circle, increasing in amplitude in the front half before decreasing in the back half. Mathematically, the advection is described by a one-parameter family of conformal maps which is a subgroup of the automorphisms of the unit disk. The important role of this subgroup has been previously established for the exactly solvable case $\epsilon = 1$ [17,18]. In Section 3.4 we discuss the anomalous behavior found at the back of the circle in the large time limit. In Section 3.5 we give arguments indicating that an initially analytic interface stays analytic for all finite times, but singularities initially outside the physical region of interest approach the back of the circle for $t \to \infty$. Provided the perturbation for $t \to \infty$ stays analytic in the closed unit disk, except for the point -1, we in Section 3.6 prove that it asymptotically reduces to a constant. This implies that the perturbation just leads to a shift in space with respect to the

[2] A correction of order $O(1/|\mathbf{x}|)$ to the electric field $\mathbf{E}$ can occur only if the streamer carries a net electric charge. We here concentrate on the analysis of streamers that are globally electrically neutral.

unperturbed propagating circle. In Section 3.7, we present numerical solutions of the linear evolution equations. These calculations support the asymptotic results derived in the previous subsections. For disturbances, not necessarily localized, we present evidence that on any part of the interface not containing a neighborhood of the bubble rear, the decay rate of the disturbance matches what is expected from the prior spectral analysis [19].

Section 4 presents a numerical study of the nonlinear evolution for different perturbations. We first consider perturbations of a circular bubble. It is shown that the circular bubble can be nonlinearly stable if the perturbation is small. However, when the perturbation is large enough, the front may start to branch. Furthermore, we study the nonlinear evolution for more general initial configurations. It is shown that the formation of a cusp precisely on the back side of the moving body cannot be excluded. We also observe that the body might split into two parts.

2. Equations resulting from conformal mapping

As already explained repeatedly [16–19], we assume the streamer to be a simply connected compact domain $\mathcal{D}$ in the (x, y)-plane. The area of $\mathcal{D}$ is conserved under the dynamics and equals π in dimensionless units. Identifying the (x, y)-plane with the closed complex plane $z = x + \mathrm{i}y$, we introduce a conformal map $f(\omega, t)$ that maps the unit disk $\mathcal{U}_\omega$ in the ω-plane to the complement of $\mathcal{D}$ in the z-plane

$$z = f(\omega, t) = \frac{a_{-1}(t)}{\omega} + \hat{f}(\omega, t), \quad a_{-1}(t) > 0. \tag{6}$$

The Laplace equation (2) and the boundary condition (5) are incorporated in the definition of a complex potential $\Phi(\omega, t)$.

$$\Phi(\omega, t) = \frac{a_{-1}(t)}{\omega} + \hat{\Phi}(\omega, t). \tag{7}$$

Both functions $\hat{f}(\omega, t)$ and $\hat{\Phi}(\omega, t)$ are analytic for $\omega \in \mathcal{U}_\omega$. The physical potential $\varphi(z, t)$ is related to $\Phi(\omega, t)$ as

$$\mathrm{Re}\ \Phi(\omega, t) = \varphi(f(\omega, t), t). \tag{8}$$

The remaining boundary conditions (1), (3) take the form

$$\mathrm{Re}\left[\frac{\partial_t f}{\omega \partial_\omega f}\right] = \mathrm{Re}\left[\frac{\omega \partial_\omega \Phi}{|\partial_\omega f|^2}\right], \quad \omega \in \partial\mathcal{U}_\omega \tag{9}$$

$$|\partial_\omega f| \mathrm{Re}\ \Phi = -\epsilon\, \mathrm{Re}\,[\omega \partial_\omega \Phi], \quad \omega \in \partial\mathcal{U}_\omega. \tag{10}$$

The problem reduces to solving these two equations, respecting the analyticity properties of f and Φ.

A simple solution corresponding to a steadily translating circle is given by

$$\begin{aligned} f^{(0)}(\omega, t) &= \frac{1}{\omega} + \frac{2t}{1+\epsilon} \\ \Phi^{(0)}(\omega, t) &= \frac{1}{\omega} - \frac{1-\epsilon}{1+\epsilon}\omega. \end{aligned} \tag{11}$$

In physical space it describes a unit circle moving with constant velocity $2/(1 + \epsilon)$ in the x-direction. For small and smooth distortions of this circle, it is appropriate to look for solutions of the form

$$\begin{aligned} f(\omega, t) &= f^{(0)}(\omega, t) + \eta\beta(\omega, t) \\ \Phi(\omega, t) &= \Phi^{(0)}(\omega, t) + \eta\frac{2}{1+\epsilon}\chi(\omega, t), \end{aligned} \tag{12}$$

where $\beta(\omega, t)$ and $\chi(\omega, t)$ are analytic in $\mathcal{U}_\omega$ and η is a small parameter. Since the area is conserved, it can be shown that the residue 1 of the pole in (11) remains unchanged to first order in η. Substituting (12) into Eqs. (9), (10) we find in first order in η a system of two partial differential equations, from which χ can be eliminated. The final equation for β takes the form

$$\mathcal{L}_\epsilon \beta = 0 \tag{13}$$

$$\mathcal{L}_\epsilon = \frac{\epsilon}{2}\partial_\omega(\omega^2 - 1)\omega\partial_\omega + \epsilon\partial_\omega\omega\partial_\tau + \partial_\tau - \partial_\omega, \tag{14}$$

where we introduced the rescaled time variable

$$\tau = \frac{2}{1+\epsilon}t. \tag{15}$$

Eqs. (13), (14) determine the linearized evolution that will be discussed in Section 3. We will assume that the initial interface is analytic, i.e., that all singularities of $\beta(\omega, 0)$ are outside the closed unit disk $\overline{\mathcal{U}_\omega}$, though much of the analysis is valid for a sufficiently smooth interface as well.[3]

3. Analysis of infinitesimal perturbations

3.1. Summary of previous results

In part I [19] we have analyzed the eigenvalue problem, resulting from Eqs. (13), (14) via the ansatz $\beta(\omega, \tau) = \mathrm{e}^{\lambda\tau}\beta_\lambda(\omega)$. We have shown that the spectrum is purely discrete and that the real part of all eigenvalues λ_n is negative, except for the trivial value $\lambda_0 = 0$, which corresponds to a simple shift of the circle. An infinite set of real negative eigenvalues was found. All eigenfunctions, except for $\beta_{\lambda_0}(\omega) = \text{const}$, are singular at $\omega = -1$ at the back of the circle. Thus the expansion of a regular initial condition in terms of eigenfunctions has to break down in the neighborhood of $\omega = -1$, which indicates that in that neighborhood some anomalous relaxation shows up. Furthermore, we found that as $\epsilon \downarrow 0$, any eigenvalue λ_n tends to zero and the corresponding eigenvector $\beta_\lambda(\omega)$ tends to a constant. A similar behavior of the spectrum was found for a steadily moving circle in a Hele–Shaw cell with surface tension regularization [22] and this degeneracy is not unexpected since the unregularized problem ($\epsilon = 0$) is mathematically ill-posed [20,21].

Here, we consider the initial value problem defined by Eqs. (13), (14). Our analysis is guided by previous results [17,18] on the special case $\epsilon = 1$ where the general time dependent solution is known analytically; it is

$$\beta(\omega, \tau) = \frac{1}{\omega^2}\int_0^\omega \omega' G\left(\frac{\omega' + T}{1 + \omega' T}\right)\mathrm{d}\omega', \tag{16}$$

where the function $G(\omega)$ is given by the initial condition,

$$G(\omega) = (2 + \omega\partial_\omega)\beta(\omega, 0), \tag{17}$$

and $T(\tau)$ is defined as

$$T(\tau) = \tanh\frac{\tau}{2}. \tag{18}$$

The properties of these solutions are discussed and visualized in detail in [17,18]. Here we in particular note that the essential time dependence of $\beta(\omega, \tau)$ is contained in the transformation

$$\zeta = \frac{\omega + T(\tau)}{1 + \omega T(\tau)}. \tag{19}$$

$\zeta(\omega, T)$, $0 \le T \le 1$, defines a one-parameter family of automorphisms of the unit disk, with fixed points $\omega = \pm 1$. The point $\omega = 1$ is stable, whereas $\omega = -1$ is unstable in the following sense: as $\tau \to \infty$, i.e. $T \to 1$, all the complex ω-plane, except for $\omega = -1$, is mapped into a neighborhood of $\zeta = +1$. This

[3] Analyticity is not crucial, except in Sections 3.5 and 3.6.

results in an advective dynamics. Any perturbation not centered precisely at $\omega = 1$ is advected towards $\omega = -1$, where it vanishes asymptotically. As $\tau \to \infty$, only a shift of the circle is left:

$$\lim_{\tau\to\infty} \beta(\omega, \tau) = \frac{G(1)}{2}. \tag{20}$$

However, it is to be noted that the limit is not uniform, and no matter how large τ is, there is a neighborhood of $\omega = -1$, where $\beta(\omega, \tau)$ may change dramatically. We note that advection of distortions from the front to the sides has been observed in viscous fingering and crystal growth models with surface tension and has been derived from somewhat heuristically simplified models [4,32]. We further note that in the limit $\epsilon \to \infty$ a purely advective dynamics results [18]:

$$\beta(\omega, \tau) = \tilde{\beta}(\zeta(\omega, T(\tau))), \qquad \epsilon = \infty.$$

Expecting the automorphism $\zeta(\omega, T)$ and the resulting advective dynamics to play an important role also for $\epsilon \neq 1$ we transform the PDE (13), (14) from variables (ω, τ) to variables (ζ, T), introducing the notation

$$\beta(\omega, \tau) = \tilde{\beta}(\zeta(\omega, T(\tau)), T(\tau)). \tag{21}$$

This results in the normal form of a hyperbolic PDE:

$$\left\{\epsilon h(\zeta, T)\partial_T\partial_\zeta + \frac{\partial h(\zeta, T)}{\partial T}\partial_\zeta + (1+\epsilon)\partial_T\right\}\tilde{\beta}(\zeta, T) = 0, \tag{22}$$

where

$$h(\zeta, T) = \frac{(\zeta - T)(1 - T\zeta)}{1 - T^2} = \omega(\zeta, T)\left[\partial_\zeta\omega(\zeta, T)\right]^{-1}. \tag{23}$$

3.2. Localized perturbations; rigorous results

We now consider some initial perturbation $\tilde{\beta}(\zeta, 0)$ localized in some small region of the unit circle and derive a rigorous result on its time dependence, Eq. (32). The detailed discussion of this result is given in Section 3.3. The analysis is limited to the unit ζ-circle which corresponds to the free boundary.

Consider for general $\epsilon > 0$ an initial perturbation that is centered at $\zeta = \zeta_c = e^{i\psi_c}$ for $\psi_c \neq 0$ and has 'width' γ in the sense that $\tilde{\beta}(e^{i\psi_c + i\gamma\chi}, 0)$ decays rapidly with $|\chi|$ when $|\chi| \gg 1$. The decay rate will be specified more precisely below Eq. (30). To study this problem, we first write (22) as an integral equation:

$$\tilde{\beta}_\zeta(\zeta, T) = \zeta^{1/\epsilon}h^{-1/\epsilon}(\zeta, T)\tilde{\beta}_\zeta(\zeta, 0) - \frac{(1+\epsilon)}{\epsilon h^{1/\epsilon}(\zeta, T)}\int_0^T \tilde{\beta}_s(\zeta, s)h^{-1+1/\epsilon}(\zeta, s)\mathrm{d}s, \tag{24}$$

where $\tilde{\beta}_\zeta$ and $\tilde{\beta}_s$ denote derivatives of $\tilde{\beta}$. Then integration by parts in s replaces $\tilde{\beta}_s$ by $\tilde{\beta}$ which is written as

$$\tilde{\beta}(\zeta, T) = \int_{\zeta_0}^{\zeta} \tilde{\beta}_\zeta(\zeta', T)\mathrm{d}\zeta' + \tilde{\beta}(\zeta_0, T).$$

Here $\zeta_0 = e^{i\psi_0}$ is a reference point in the tail of the perturbation chosen such that $0 < \psi_0 < \psi_c \leq \pi$. We assume that $\frac{\psi_c - \psi_0}{\gamma}$ is so large that $\tilde{\beta}(\zeta_0, 0)$ is negligible.

Then, after some algebraic manipulation, we are able to rewrite (24) as the following equation for

$$\hat{G}(\chi, T) \equiv \tilde{\beta}_\zeta\left(e^{i\psi_c + i\gamma\chi}, T\right) \tag{25}$$

$$\begin{aligned}\hat{G}(\chi, T) &= \hat{G}^{(0)}(\chi, T) + \int_0^T \int_{-\frac{\psi_c-\psi_0}{\gamma}}^{\chi} \mathcal{K}_1(\chi, \chi', T, s) \\ &\quad \times \hat{G}(\chi', s)\mathrm{d}\chi'\mathrm{d}s + \int_{-\frac{\psi_c-\psi_0}{\gamma}}^{\chi} \mathcal{K}_2(\chi, \chi', T)\hat{G}(\chi', T)\mathrm{d}\chi' \\ &\equiv \hat{G}^{(0)}(\chi, T) + \mathcal{L}\left[\hat{G}\right](\chi, T),\end{aligned} \tag{26}$$

where, with the understanding that $\zeta = e^{i\psi_c + i\gamma\chi}$, $\zeta' = e^{i\psi_c + i\gamma\chi'}$,

$$\begin{aligned}\mathcal{K}_1(\chi, \chi', T, s) &= \frac{i\gamma\zeta'(1-\epsilon^2)(1-T^2)^{1/\epsilon}}{\epsilon^2\{(\zeta - s)(1 - \zeta s)\}^{1/\epsilon}} \\ &\quad \times \left(\frac{(\zeta - s)(1 - s\zeta)}{(1 - s^2)}\right)^{-1+1/\epsilon} \\ &\quad \times \left[\frac{1}{s - \zeta} + \frac{\zeta}{s\zeta - 1} - \frac{2s}{s^2 - 1}\right],\end{aligned} \tag{27}$$

$$\mathcal{K}_2(\chi, \chi', T) = -i\gamma\zeta'\frac{(1+\epsilon)(1-T^2)}{\epsilon(\zeta - T)(1 - T\zeta)}, \tag{28}$$

and

$$\begin{aligned}\hat{G}^{(0)}(\chi, T) &= h^{-1/\epsilon}(\zeta, T)\zeta^{1/\epsilon}\tilde{\beta}_\zeta(\zeta, 0) \\ &\quad - \frac{(1+\epsilon)\tilde{\beta}(\zeta_0, T)}{\epsilon h(\zeta, T)} + \frac{(1+\epsilon)\tilde{\beta}(\zeta, 0)\zeta^{1/\epsilon}}{\epsilon\zeta h^{1/\epsilon}(\zeta, T)} \\ &\quad + \frac{(1-\epsilon^2)}{\epsilon^2 h^{1/\epsilon}(\zeta, T)}\int_0^T h^{-2+1/\epsilon}(\zeta, s)h_T(\zeta, s)\tilde{\beta}(\zeta_0, s)\mathrm{d}s.\end{aligned} \tag{29}$$

With $\hat{G}^{(0)}(\chi, T)$ considered known[4] we determine the solution $\hat{G}(\chi, T)$ to the integral equation (26) for $\chi \in \left[-\frac{\psi_c - \psi_0}{\gamma}, \chi_R\right]$, $T \in [0, T_0]$, where χ_R and $T_0 < 1$ are some suitably chosen positive values independent of γ. Now it is clear from the expression for $\mathcal{K}_1$ and $\mathcal{K}_2$ that they are uniformly small in the $\|.\|_\infty$ norm when $\frac{\gamma}{\epsilon^2}$ is sufficiently small. We now choose the norm

$$\|\hat{G}\| \equiv \sup_{T\in[0,T_0]} \sup_{\chi\in\left[-\frac{\psi_c-\psi_0}{\gamma}, \chi_R\right]} W(\chi)|\hat{G}(\chi, T)|, \tag{30}$$

where the positive weight function $W(\chi)$ obeys

$$W(\chi)\int_{-\infty}^{\chi_R} W^{-1}(\chi')\mathrm{d}\chi' < C < \infty \quad \chi \leq \chi_R.$$

For example, $W(\chi) = e^{-\chi}$ for $\chi \leq 0$ and 1 for $\chi > 0$ would suffice for our analysis. We define $\hat{G}$ to be localized if $\|\hat{G}\|$ is finite, and ζ_0, T_0 can be chosen such that $\tilde{\beta}(\zeta_0, T)$ is negligibly small for $T \in [0, T_0]$. Now it is clear from (26) that the linear operator $\mathcal{L}$ has the contracting property

$$\|\mathcal{L}[\hat{G}_1 - \hat{G}_2]\| \leq C\frac{\gamma}{\epsilon^2}\|\hat{G}_1 - \hat{G}_2\|. \tag{31}$$

It follows that there exists a unique solution to the integral equation (26) if γ/ϵ^2 is small enough and that for $\gamma/\epsilon^2 \ll 1$

$$\hat{G}(\chi, T) \sim \hat{G}^{(0)}(\chi, T),$$

provided χ and T are in the above specified range. For a perturbation localized in the sense given above, our result reduces to

$$\hat{G}(\chi, T) \sim h^{-1/\epsilon}\left(e^{i\psi_0}, T\right)\tilde{\beta}_\zeta\left(e^{i(\psi_0 + \gamma\chi)}, 0\right). \tag{32}$$

We note that $\mathcal{L}[\hat{G}](\chi, T)$ in general will not vanish for $\chi \to \infty$. This is the reason for restricting χ to the interval given above and indicates that for $T > 0$ the localized perturbation will sit on top of a dynamically generated delocalized background of amplitude $\sim \gamma/\epsilon^2$.

A detailed discussion of the result (32) will be presented in the next subsection.

[4] Since $\tilde{\beta}(\zeta_0, T)$ cannot be determined without considering the full non-local problem on $|\zeta| = 1$, part of the expression (29) for $\hat{G}^{(0)}$ is not known. Nonetheless, if a disturbance is localized, the contribution to $\hat{G}^{(0)}$ from $\tilde{\beta}(\zeta_0, T)$ will be relatively small. In any case, in order to study the evolution in the χ-scale, we are not prevented from considering $\hat{G}^{(0)}$ as known.

3.3. Localized perturbations; formal intuitive arguments

It is useful to obtain the result (32) through a more formal, yet intuitive, reasoning. This will also be helpful in our subsequent treatment of the long-time asymptotics in the anomalous region near the back of the bubble. We again restrict the analysis to the unit circle $\omega = e^{i\alpha}$, $\alpha \in \mathbb{R}$, or correspondingly to $\zeta = e^{i\psi}$, $\psi \in \mathbb{R}$. According to Eq. (19), the two angular coordinates α and ψ are related through

$$\alpha = \arctan \frac{\left(1 - T^2\right) \sin \psi}{\left(1 + T^2\right) \cos \psi - 2T}. \tag{33}$$

Initially (at $T = 0$), α and ψ obviously are identical. In terms of ψ, the PDE (22) takes the form

$$\left\{ \epsilon \hat{h}(\psi, T) \partial_T \partial_\psi + \frac{\partial \hat{h}(\psi, T)}{\partial T} \partial_\psi + i(1+\epsilon)\partial_T \right\} \times \tilde{\beta}\left(e^{i\psi}, T\right) = 0, \tag{34}$$

where

$$\hat{h}(\psi, T) = \left(\partial_\psi \alpha\right)^{-1} = \frac{(1-T)^2 + 4T \sin^2 \psi/2}{1 - T^2}. \tag{35}$$

We now search for a solution that during its evolution stays localized near a fixed angle ψ_c, with an angular width $\gamma \ll \pi$. We use the ansatz

$$\tilde{\beta}\left(e^{i\psi}, T\right) = \tilde{\beta}_{\text{loc}}(\chi, T), \tag{36}$$

where again

$$\chi = \frac{\psi - \psi_c}{\gamma}, \tag{37}$$

and $\tilde{\beta}_{\text{loc}}(\chi, T)$ is assumed to vanish rapidly for $|\chi| > 1$. With this ansatz, Eq. (34) takes the form

$$\Big[\epsilon \hat{h}(\psi_c + \gamma\chi, T) \partial_T \partial_\chi + \left(\partial_T \hat{h}(\psi_c + \gamma\chi, T) \right) \partial_\chi + i\gamma(1+\epsilon)\partial_T \Big] \cdot \tilde{\beta}_{\text{loc}}(\chi, T) = 0. \tag{38}$$

For $\gamma \ll \pi$ we neglect the term $i\gamma(1+\epsilon)\partial_T$ and the χ-dependence in the argument of $\hat{h}$ to find an approximate solution of the form

$$\tilde{\beta}_{\text{loc}}(\chi, T) = \hat{h}^{-1/\epsilon}(\psi_c, T) \tilde{\beta}_{\text{loc}}(\chi, 0), \tag{39}$$

which is the same as (32).

Before we evaluate this result we briefly discuss its limitations that result from the present derivation. In view of the assumptions $\gamma \ll \pi$, and $|\chi| \lesssim 1$, the use of the zero order result $\hat{h}(\psi) \approx \hat{h}(\psi_c)$ is justified provided

$$(1-T)^2 + 4T \sin^2 \frac{\psi_c}{2} \gg 2T\gamma\chi \sin \psi_c + T(\gamma\chi)^2 \cos \psi_c. \tag{40}$$

This is valid for all times provided $|\psi_c| \gg \gamma$, i.e., for initial conditions $\tilde{\beta}_{\text{loc}}(\chi, 0)$ which essentially vanish in the forward direction $\psi = 0$. For $\psi_c \approx 0$ the condition (40) is violated if $(1 - T)$ becomes of the order γ, and therefore the approximation becomes invalid in the large-time limit $T(\tau) \to 1$. This special role of perturbations in the forward direction is not unexpected since for such perturbations advection is ineffective.

Neglecting the term $\sim i\gamma(1+\epsilon)\partial_T$ has more serious consequences. Substituting into Eq. (38) an ansatz of the form

$$\tilde{\beta}_{\text{loc}}(\chi, T) = \tilde{\beta}^{(0)}(\chi, T) + \gamma \tilde{\beta}^{(1)}(\chi, T) + \mathcal{O}(\gamma^2)$$

one finds that the result for $\tilde{\beta}^{(1)}$ violates the condition $\tilde{\beta}^{(1)}(\chi, T) \approx 0$ for $|\chi| \gg 1$. A localized initial condition dynamically generates a delocalized contribution, with an amplitude proportional to γ/ϵ^2, in full accord with the rigorous discussion of the previous subsection. Again this result is not unexpected since the eigenfunctions of the operator $\mathcal{L}_\epsilon$, Eq. (14), are delocalized. Assuming that we can expand an initially localized perturbation in terms of eigenfunctions we must expect that the balance of the expansion coefficients $a_n e^{\lambda_n \tau}$, which for $\tau = 0$ leads to localization, is destroyed by the time evolution. With these limitations in mind, we now discuss the result (39).

According to Eq. (39), if expressed in the variable $\zeta = \exp(i(\psi_c + \gamma\chi))$ the evolution of the perturbation is most simple. Neither its position ψ_c nor its shape $\hat{\beta}_{\text{loc}}(\chi, 0)$ change. Only the overall amplitude $\hat{h}^{-1/\epsilon}$ varies with time. For $0 < |\psi_c| < \pi/2$, i.e., if ψ_c is at the front half of the circle, $\hat{h}^{-1/\epsilon}$ increases up to a time τ_m given by

$$\left(T^2(\tau_m) + 1\right) \cos \psi_c - 2T(\tau_m) = 0, \tag{41}$$

and then decreases again. For $|\psi_c| > \pi/2$, $\hat{h}^{-1/\epsilon}$ decreases monotonically. For any $\psi_c \neq 0$, we find the asymptotic behavior

$$\hat{h}^{-1/\epsilon}(\psi_c, T(\tau)) \sim \frac{e^{-\tau/\epsilon}}{\sin^2 \psi_c/2} \quad \text{for } \tau \to \infty. \tag{42}$$

For a perturbation centered precisely at the back of the circle ($\psi_c = \pi$), exponential relaxation

$$\hat{h}^{-1/\epsilon}(\pi, T(\tau)) = \left(\frac{1-T}{1+T}\right)^{1/\epsilon} = e^{-\tau/\epsilon} \tag{43}$$

holds for all τ. We recall that the localized approximation must break down if $\hat{h}^{-1/\epsilon}$ becomes of the order of the amplitude of the delocalized background. Nevertheless we will argue in Section 3.4 that a contribution with asymptotic time behavior $e^{-\tau/\epsilon}$ generally shows up.

Using Eq. (33) to transform back to $\omega = e^{i\alpha}$ we see that the center $\alpha_c(T(\tau))$ is convected along the circle, reaching $\pm\pi$ for $\tau \to \infty$. A little calculation yields the velocity of this advection

$$\frac{d}{d\tau} \alpha_c(T(\tau)) = \sin \alpha_c(T(\tau)). \tag{44}$$

This result has a simple interpretation. Recalling that we are working in a frame moving with the velocity $\mathbf{v} = \dot{\mathbf{x}}$ of the unperturbed circle, we identify the velocity (44) as the projection of $\mathbf{v}$ onto the tangent to the circle at the instantaneous location of the perturbation.

In terms of α_c the overall amplitude of the perturbation takes the simple form

$$\hat{h}^{-1/\epsilon} = \left(\frac{\sin \alpha_c(T(\tau))}{\sin \alpha_c(0)} \right)^{1/\epsilon}. \tag{45}$$

It increases as long as the perturbation is on the front half of the circle and decreases on the back side. The maximum, reached for $\alpha_c(T(\tau)) = \pm\pi/2$, strongly depends on the initial position $\alpha_c(0) \equiv \psi_c$.

Defining the scale factor of the width of the perturbation as

$$\Gamma = \left. \frac{\partial \alpha}{\partial \psi} \right|_{\psi = \psi_c} \tag{46}$$

we find

$$\Gamma = \hat{h}^{-1}(\psi_c, T(\tau)) = \frac{\sin \alpha_c(T(\tau))}{\sin \alpha_c(0)}. \tag{47}$$

Thus the width behaves similarly to the amplitude, except that for $\epsilon \ll 1$ it varies much less. For $\tau \to \infty$ it vanishes like $e^{-\tau}$.

So far we considered perturbations localized away from the tip $\psi_c = 0 = \alpha_c(0)$ of the circle. For $\psi_c = 0$, Eq. (39) still holds for times such that

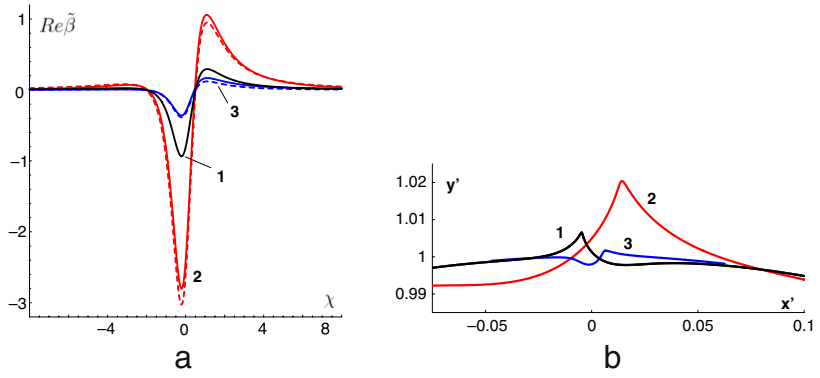

Fig. 2. Evolution of a strongly localized perturbation for $\epsilon = 1$. Curves 1, 2 and 3 correspond to times $\tau = 0$, 1.84 and 4.59, respectively. (a) Re $\tilde{\beta}$ as function of the comoving angular coordinate $\chi = (\psi - \psi_c)/\gamma$. Broken lines: local approximation. Full lines: exact result with the shift of the circle subtracted. (b) Perturbed interface in the physical plane in the system of local tangential and normal coordinates as explained in the text.

$$1 - T(\tau) \gg \gamma,$$

cf. Eq. (40). It describes the initial increase and broadening of the perturbation. Advection, of course, is absent. For $1 - T \approx \gamma$ the width becomes of order 1 and the local approximation clearly becomes invalid.

On the qualitative level these results are most similar to the exact results found for $\epsilon = 1$ [17,18] and resemble the dynamics of a localized perturbation found in the context of viscous fingering [32].

The quantitative performance of the local approximation is illustrated in Fig. 2, where for $\epsilon = 1$ the exact evolution of a localized perturbation is compared to our approximation. From the exact result (16) the contribution $G(T)/2$ representing a simple shift of the circle, has been subtracted. The initial condition is chosen as

$$\tilde{\beta}(\mathrm{e}^{\mathrm{i}\psi}, 0) = \frac{\gamma^2}{\left(\mathrm{e}^{\mathrm{i}\psi} - (1+\gamma)\,\mathrm{e}^{\mathrm{i}\psi_c}\right)^2}$$

with

$$\psi_c = -\frac{\pi}{10}, \qquad \gamma = \frac{1}{200}.$$

Fig. 2(a) shows Re $\tilde{\beta}$ as a function of $\chi = (\psi - \psi_c)/\gamma$ for three different times. Curve 1 shows the initial condition, where by construction the exact form and the approximation coincide. Curve 2 shows the perturbation when it is largest, in ω-space being located near $\omega = -\mathrm{i}$. Curve 3 is taken at some later time. Evidently in this example the local approximation (broken lines) is quite accurate. Very similar results are found for Im $\tilde{\beta}$, which therefore is not shown. Fig. 2(b) shows the effect of this perturbation in physical space. In evaluating $z = f(\omega, t)$, Eq. (12), we choose the amplitude $\eta = 0.007\mathrm{e}^{-\mathrm{i}\psi_c}$. To combine the three curves into one plot, we introduced a time-dependent rotation of the coordinate system such that y' or x' are measured along the normal or the tangent to the unperturbed circle at the center of the perturbation, (i.e., at angle $-\alpha_c(T(\tau))$, since the inversion contained in the conformal map induces a sign change of the angles). In this representation the exact solution and the approximation cannot be distinguished within the resolution of the plot. We note that in physical space the shape of the perturbation varies due to interference with the unperturbed circle.

3.4. Asymptotic relaxation near $\omega = -1$

The analysis presented in Sections 3.2 and 3.3 clearly demonstrates the advection of an initially localized disturbance towards $\omega = -1$, corresponding to the rear of the bubble. Note that Eqs. (18) and (19) mean that any fixed $\zeta \neq 1$ maps to $\omega = -1$ as $\tau \to +\infty$, i.e., as $T \to 1^-$. We now consider the relaxation process at $\omega = -1$ for large time τ.

In discussing the asymptotic relaxation we prefer to rewrite (22) in terms of τ, using $(1 - T^2)\partial_T = 2\partial_\tau$. Inserting the explicit form (23) of $h(\zeta, T)$ and multiplying by $(1 - T^2)^2/2$ we find

$$\left[\epsilon(\zeta - T)(1 - T\zeta)\partial_\tau\partial_\zeta + \left(2T\zeta - \frac{1}{2}(1+T^2)(1+\zeta^2)\right)\partial_\zeta + (1+\epsilon)(1-T^2)\partial_\tau\right]\tilde{\beta}(\zeta, T) = 0. \tag{48}$$

Here T stands for

$$T = T(\tau) = \tanh\tau/2 = 1 - 2\mathrm{e}^{-\tau} + \mathcal{O}\left(\mathrm{e}^{-2\tau}\right),$$

cf. Eq. (18). Keeping only the leading τ-dependence in the coefficients of the derivatives, we reduce Eq. (48) to

$$\left[-(\epsilon\partial_\tau + 1)(1-\zeta)^2\partial_\zeta + 4(1+\epsilon)\,\mathrm{e}^{-\tau}\partial_\tau\right]\tilde{\beta}(\zeta, T(\tau)) = 0. \tag{49}$$

For $\tau \gg 1$ we neglect the term $\mathrm{e}^{-\tau}\partial_\tau\tilde{\beta}$ to find

$$\tilde{\beta}(\zeta, T(\tau)) \sim \mathrm{e}^{-\tau/\epsilon}\hat{\beta}_0(\zeta) + \gamma_0, \tag{50}$$

where $\hat{\beta}_0(\zeta)$ and γ_0 depend on the initial condition $\tilde{\beta}(\zeta, 0)$ and of course cannot be fixed by this asymptotic argument.

Since the derivative ∂_ζ in Eq. (49) is multiplied by $(1 - \zeta)^2$, the neglect of the term involving $\mathrm{e}^{-\tau}\partial_\tau$ can be justified only for $\zeta \neq +1$. In terms of

$$\omega = \frac{\zeta - T}{1 - T\zeta} = -1 + 2\frac{1+\zeta}{1-\zeta}\,\mathrm{e}^{-\tau} + \mathcal{O}\left(\mathrm{e}^{-2\tau}\right) \tag{51}$$

this implies that we deal with a neighborhood of $\omega = -1$ that is contracted to this point like $\mathrm{e}^{-\tau}$. This range of ω is complementary to the region where an expansion in terms of eigenfunctions can be expected to be valid asymptotically.

In the result (50) the ζ-dependence is suppressed by a factor $\mathrm{e}^{-\tau/\epsilon}$, which for $\epsilon \ll 1$, $\tau \to \infty$, vanishes much faster than $\mathrm{e}^{-\tau}$. Thus ζ-dependent corrections of order $\mathrm{e}^{-\tau}$ will dominate the asymptotic relaxation at the back of the circle. Noting the presence of $\mathrm{e}^{-\tau}$ in the coefficients of the differential equation, it is natural to determine the structure of these terms with the ansatz

$$\tilde{\beta}\,(\zeta, T(\tau)) = \mathrm{e}^{-\tau/\epsilon}\hat{\beta}(\zeta, \tau) + \hat{\gamma}(\zeta, \tau), \tag{52}$$

where

$$\hat{\gamma}(\zeta, \tau) = \sum_{k=0}^{\infty}\hat{\gamma}_k(\zeta)\,\mathrm{e}^{-k\tau}. \tag{53}$$

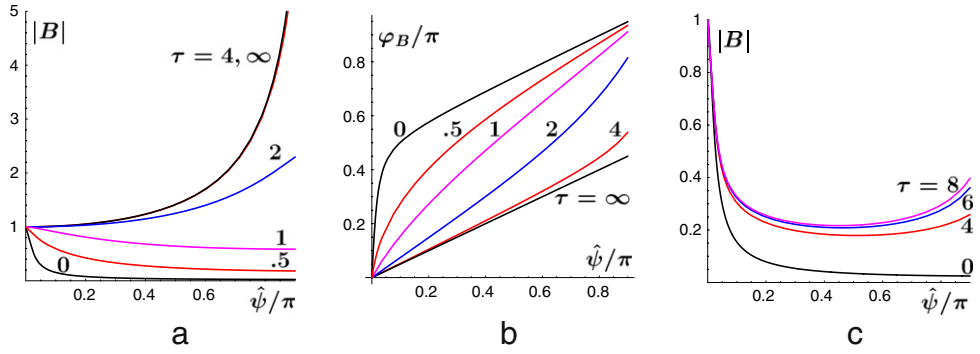

Fig. 3. Time evolution of the initial condition (59). (a) $|B(\hat\psi,\tau)|$ as a function of $\hat\psi/\pi$ for times τ as given and for $\epsilon = 0.1$. (b) Phase of B for the same values of τ and ϵ. (c) Again $|B(\hat\psi,\tau)|$ as a function of $\hat\psi/\pi$, but now for $\epsilon = 0.8$.

From Eq. (48) with $\tilde\beta(\zeta, T(\tau))$ replaced by $\hat\gamma(\zeta,\tau)$ we find

$$\hat\gamma(\zeta,\tau) = \hat c_0 + \hat c_1\, \mathrm{e}^{-\tau} + \left(\hat c_2 - \frac{1+\epsilon}{1-2\epsilon}\frac{4\hat c_1}{1-\zeta}\right)\mathrm{e}^{-2\tau} + \left(\hat c_3 - \frac{1+\epsilon}{1-3\epsilon}\frac{8\hat c_2}{1-\zeta} + \frac{(1+\epsilon)^2}{(1-2\epsilon)(1-3\epsilon)} \times \frac{16\hat c_1}{(1-\zeta)^2}\right)\mathrm{e}^{-3\tau} + \mathcal{O}\left(\mathrm{e}^{-4\tau}\right), \tag{54}$$

where the $\hat c_k$ are integration constants. Generally $\hat\gamma_k(\zeta)$ is found to be a polynomial in $(1-\zeta)^{-1}$ of degree $k-1$. In this analysis we assumed $\epsilon \neq 1/n$. For $\epsilon = 1/n$ the ansatz (53) has to be modified. In particular a term proportional to $\tau \mathrm{e}^{-n\tau}$ has to be included. We note that the exact result for $\epsilon = 1$ shows such a contribution [18].

To transform our result back to ω-space we introduce

$$\delta\omega = (1+\omega)\,\mathrm{e}^{\tau}, \tag{55}$$

$$\gamma(\delta\omega,\tau) = \hat\gamma\left(\zeta(\delta\omega),\tau\right) - \hat\gamma(-1,\tau). \tag{56}$$

Eq. (19) yields

$$\frac{1}{1-\zeta} = \frac{1+\frac{T}{1+T}\delta\omega}{2-\delta\omega\mathrm{e}^{-\tau}} = \frac{1}{2} + \frac{1}{4}\delta\omega + \mathcal{O}(\mathrm{e}^{-\tau}). \tag{57}$$

Thus $\gamma(\delta\omega,\tau)$ has an expansion of the form

$$\gamma(\delta\omega,\tau) = \mathrm{e}^{-\tau}\sum_{k=1}^{\infty} c_k\left(\delta\omega\mathrm{e}^{-\tau}\right)^k\left[1+\mathcal{O}\left(\mathrm{e}^{-\tau}\right)\right], \tag{58}$$

where the c_k again depend on the initial condition. For $\epsilon \ll 1$ the terms of order $k < 1/\epsilon - 1$ dominate over the contribution $\mathrm{e}^{-\tau/\epsilon}\hat\beta$. For $\epsilon < 1/2$ we therefore in a region of size $|1+\omega| = \mathcal{O}\left(\mathrm{e}^{-\tau}\right)$ near $\omega = -1$ expect to see a very smooth asymptotic relaxation of the interface, with only a few coefficients depending on the initial condition. In contrast, for $\epsilon > 1/2$ the asymptotic relaxation is determined by the term $\mathrm{e}^{-\tau/\epsilon}\hat\beta_0(\zeta)$, which will depend on the initial condition in a complicated way. For $\epsilon = 1$ this is illustrated in Fig. 5.2 of Ref. [18]. In the next subsection we will argue that the function $\hat\beta_0(\zeta)$ picks up contributions due to singularities of the initial condition, which for $\tau \to \infty$ are driven towards $\omega = -1$. We finally note that the results discussed here resemble the behavior of the low order eigenfunctions $\beta_\lambda(\omega)$. As shown in part I [19] of this series of papers, these functions near $\omega = -1$ develop a singularity of the form $(1+\omega)^{1/\epsilon+\lambda}$, implying that the derivatives at $\omega = -1$ exist for all orders $k < 1/\epsilon + \lambda$.

To illustrate our results we consider a perturbation centered at $\omega = -1$. As the initial condition we choose

$$\tilde\beta(\zeta,0) = \frac{\gamma}{\gamma-\zeta}, \quad \gamma = 1.05, \tag{59}$$

and we calculate the function

$$B(\hat\psi,\tau) = \frac{\tilde\beta(-\mathrm{e}^{\mathrm{i}\hat\psi},T(\tau)) - \tilde\beta(0,T(\tau))}{\tilde\beta(-1,T(\tau)) - \tilde\beta(0,T(\tau))}. \tag{60}$$

We expect to find the limiting behavior

$$B(\hat\psi,\tau) \xrightarrow[\tau\to\infty]{} \frac{1}{1+\mathrm{e}^{\mathrm{i}\hat\psi}} - 1 = \frac{\mathrm{e}^{\mathrm{i}\hat\psi/2}}{\cos\hat\psi/2}, \quad \epsilon < \frac{1}{2}, \tag{61}$$

or

$$B(\hat\psi,\tau) \xrightarrow[\tau\to\infty]{} \frac{\hat\beta_0(-\mathrm{e}^{\mathrm{i}\hat\psi}) - \hat\beta_0(0)}{\hat\beta_0(-1) - \hat\beta_0(0)}, \quad \epsilon > \frac{1}{2}, \tag{62}$$

respectively. Whereas $\hat\beta_0(\zeta)$ depends on the initial condition, the limit (61) is universal. The results shown in Fig. 3 conform to these expectations.

Fig. 3(a) shows $|B(\hat\psi,\tau)|$ for several values of τ and for $\epsilon = 0.1$. It illustrates the approach to the limiting form $1/\cos(\hat\psi/2)$, which within the accuracy of the plot is in fact reached for $\tau \approx 4$. Fig. 3(b) shows the corresponding phase of $B(\hat\psi,\tau)$. Here the approach to the limit is slower, but is definitely visible. Fig. 3(c) shows results for $|B(\hat\psi,\tau)|, \epsilon = 0.8$. Here $|B(\hat\psi,\tau)|$ seems to approach a limiting curve which clearly shows remainders of the initial peak. (We should note that $B(\hat\psi,\tau)$ is symmetric: $B(-\hat\psi,\tau) = B^*(\hat\psi,\tau)$, and that the peak at $\hat\psi = 0$, of course, is rounded, which however is not visible on the scale of the plot.) We finally recall that the $\hat\psi$-range shown here in terms of $\omega = \mathrm{e}^{\mathrm{i}\alpha}$ corresponds to a small region near $\alpha = \pi$. Specifically for $\tau = 4$ it corresponds to $\pi \le \alpha \le 1.08\pi$.

For the asymptotic relaxation our results predict

$$\tilde\beta(\zeta,T(\tau)) \sim \begin{cases} \mathrm{e}^{-2\tau}, & \epsilon < \frac{1}{2} \\ \mathrm{e}^{-\tau/\epsilon}, & \epsilon > \frac{1}{2} \end{cases} \quad \text{for } \tau \to \infty. \tag{63}$$

This prediction is tested in Fig. 4 by plotting results for $\ln[\tilde\beta(-1,T(\tau)) - \tilde\beta(0,T(\tau))]$ as a function of τ for several values of ϵ. The expected behavior is reasonably well observed.

3.5. Analyticity of the interface

If we assume the initial interface to be analytic, all singularities of the initial perturbation $\beta(\omega,0)$ have to be outside the closed unit disk, $\overline{\mathcal{U}}_\omega$. We here argue that under the linearized dynamics the singularities stay outside $\overline{\mathcal{U}}_\omega$ for all finite times τ. For $\tau \to \infty$ they approach $\omega = -1$, and contribute to the anomalous $\mathrm{e}^{-\tau/\epsilon}\hat\beta(\zeta)$ behavior found in Section 3.4.

This argument is based on the recurrence relation for the coefficients $b_k(\tau)$ in the Taylor expansion

$$\beta(\omega,\tau) = \sum_{k=0}^{\infty} b_k(\tau)\omega^k. \tag{64}$$

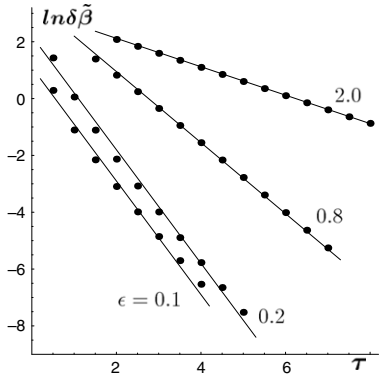

Fig. 4. $\ln[\tilde{\beta}(-1, T(\tau)) - \tilde{\beta}(0, T(\tau))]$ as a function of τ for several values of ϵ. The initial condition is given in (59). The lines indicate the expected slope -2 for $\epsilon < 1/2$ or $-1/\epsilon$ for $\epsilon > 1/2$, respectively.

The evolution equation (13), (14) yields

$$2\partial_\tau b_0 = \frac{2+\epsilon}{1+\epsilon} b_1, \tag{65}$$

$$2\partial_\tau b_k = \frac{k+1}{1+\epsilon+\epsilon k}\Big[(2+\epsilon+\epsilon k) b_{k+1} - \epsilon(k-1) b_{k-1}\Big] \quad \text{for } k \geq 1.$$

The singularities of $\beta(\omega, \tau)$ are determined by the behavior of the $b_k(\tau)$ in the limit $k \to \infty$. For simplicity, we consider an initial condition $\beta(\omega, 0)$ whose singularity closest to $|\omega| = 1$ is a branch point at ω_0 with behavior $\beta(\omega, 0) \sim \text{const}(\omega_0 - \omega)^{\alpha-1}$ for nonintegral α or a pole with α a non-positive integer. Then $b_k(0)$ for $k \gg 1$ behaves as

$$b_k(0) = \text{const}\, \omega_0^{-k} k^{-\alpha} \left(1 + \mathcal{O}\left(\frac{1}{k}\right)\right).$$

We therefore make the ansatz

$$b_k(\tau) = (-1)^k \mathrm{e}^{-kf(\tau)} g(\tau) k^{-\alpha} \left[1 + \frac{1}{k}\Delta(\tau) + \mathcal{O}\left(\frac{1}{k^2}\right)\right], \tag{66}$$

where the factor $(-1)^k$ is introduced since we expect the point $\omega = -1$ to play a special role. We will find that this ansatz is internally consistent provided $k \gg k_0$, where k_0 increases with τ. We shall conclude that for any $\tau > 0$,

$$|\mathrm{e}^{-f(\tau)}| < 1, \tag{67}$$

if this condition is satisfied initially. This implies that the singularity remains outside the unit disk for all times and suggests that at least for initial conditions with a branch point, the interface will remain analytic.

Substituting the ansatz (66) into the recurrence relation (65), we find

$$\left(-2\partial_\tau f + \mathrm{e}^{-f} - \mathrm{e}^{f}\right)\left(1 + \frac{\Delta}{k}\right) + \frac{1}{k}\left[2\partial_\tau \ln g + \left(\frac{1}{\epsilon} + 1 - \alpha\right)\left(\mathrm{e}^{f} + \mathrm{e}^{-f}\right)\right] = \mathcal{O}\left(\frac{1}{k^2}\right). \tag{68}$$

The leading order yields

$$2\partial_\tau f = \mathrm{e}^{-f} - \mathrm{e}^{f},$$

with the solution

$$f(\tau) = \ln \frac{1 - C\mathrm{e}^{-\tau}}{1 + C\mathrm{e}^{-\tau}}, \tag{69}$$

where C is some integration constant. $g(\tau)$ is determined by the next order:

$$g(\tau) = g(0)\, \mathrm{e}^{\left(\alpha-1-\frac{1}{\epsilon}\right)\tau} \left(1 - C^2\, \mathrm{e}^{-2\tau}\right)^{\alpha-1-\frac{1}{\epsilon}}. \tag{70}$$

Checking higher orders in an expansion in powers of $1/k$, one finds that neglecting such terms assumes $k \gg \frac{\mathrm{e}^{\tau}}{\epsilon} = k_0$. Combining our results we find the asymptotic behavior

$$b_k(\tau) \sim (-1)^k \left(\frac{1 + C\,\mathrm{e}^{-\tau}}{1 - C\,\mathrm{e}^{-\tau}}\right)^k g(0)\, \mathrm{e}^{\left(\alpha-1-\frac{1}{\epsilon}\right)\tau} \times \left(1 - C^2\,\mathrm{e}^{-2\tau}\right)^{\alpha-1-\frac{1}{\epsilon}} k^{-\alpha}. \tag{71}$$

Regularity of the initial condition enforces

$$\left|\mathrm{e}^{-f(0)}\right| = \left|\frac{1+C}{1-C}\right| < 1,$$

equivalent to $\mathrm{Re}\, C < 0$. With the form (69) of $f(\tau)$ this guarantees that condition (67), $|\mathrm{e}^{-f(\tau)}| < 1$, is fulfilled for all finite τ. Thus for $\tau < \infty$ the singularities of $\beta(\omega, \tau)$ stay at some finite distance from the unit disk and the interface stays smooth. $f(\tau)$ vanishes for $\tau \to \infty$, indicating that a singularity reaches $\omega = -1$.

In the above ansatz (66), we assumed a particular type of branch point or a pole for $\beta(\omega, 0)$ as the nearest singularity. Multiple singularities of this type can be accommodated in this linear analysis using the superposition principle. Other singularities can be accommodated as well by replacing $k^{-\alpha}$ by a more general k dependence.

We now consider the limiting behavior of $b_k(\tau)$ for $\tau \to \infty$ more closely. Eq. (71) yields

$$b_k(\tau) \sim (-1)^k \exp\left[2Ck\,\mathrm{e}^{-\tau}\right] g(0) \left(k\,\mathrm{e}^{-\tau}\right)^{1+\frac{1}{\epsilon}-\alpha} k^{1-\frac{1}{\epsilon}}. \tag{72}$$

This result, however, for $\tau \to \infty$ is only valid for

$$\eta = k\,\mathrm{e}^{-\tau} \gg 1, \tag{73}$$

i.e., for extremely large k. To extend the analysis to values $\eta = k\,\mathrm{e}^{-\tau} = \mathcal{O}(1)$ we make the ansatz

$$b_k(\tau) \sim (-1)^k k^{-\frac{1}{\epsilon}-1} \tilde{g}(\eta, \tau), \tag{74}$$

which is motivated by Eq. (72). The recurrence relation (65) takes the form

$$\begin{aligned}(2\partial_\tau - 2\eta\partial_\eta)\tilde{g}(\eta, \tau) &= \left(k + \mathcal{O}\left(\frac{1}{k}\right)\right)\tilde{g}\left(\eta - \mathrm{e}^{-\tau}, \tau\right) \\ &\quad - \left(k + \mathcal{O}\left(\frac{1}{k}\right)\right)\tilde{g}\left(\eta + \mathrm{e}^{-\tau}, \tau\right) \\ &= -2k\,\mathrm{e}^{-\tau}\partial_\eta \tilde{g}(\eta, \tau) + \mathcal{O}\left(\frac{1}{k}\right) \\ &= -2\eta\partial_\eta \tilde{g}(\eta, \tau) + \mathcal{O}\left(\frac{1}{k}\right),\end{aligned}$$

or

$$2\partial_\tau \tilde{g}(\eta, \tau) = \mathcal{O}\left(\frac{1}{k}\right), \tag{75}$$

equivalently. Thus to leading order in $1/k$, $\tilde{g}(\eta, \tau)$ is independent of τ and Eq. (61) reduces to

$$b_k(\tau) \sim (-1)^k k^{-\frac{1}{\epsilon}-1} \tilde{g}_0\left(k\,\mathrm{e}^{-\tau}\right). \tag{76}$$

Inspecting the terms of order $1/k$ one finds that this result asymptotically should be valid for $\mathrm{e}^{-\tau} \ll 1$ and $k \gtrsim \mathrm{e}^{\tau}/\epsilon^2$.

The $b_k(\tau)$, Eq. (76), can be interpreted as coefficients of a Taylor expansion with respect to ω of the function $\hat{\beta}_0(\zeta(\omega, T))$ introduced in the previous subsection, cf. Eq. (50). To show this we again introduce $\delta\omega$

$$\omega = -1 + \delta\omega\, \mathrm{e}^{-\tau}$$

as defined in Eq. (55), and we approximately resum the Taylor expansion from $k = \eta_0 \mathrm{e}^{\tau}$ to infinity, using the result (76).

$$\sum_{k=\eta_0 e^{\tau}}^{\infty} b_k(\tau)\left(-1+\delta\omega\, e^{-\tau}\right)^k \approx \int_{\eta_0 e^{\tau}}^{\infty} dk\, k^{-\frac{1}{\epsilon}-1}\tilde{g}_0(k\, e^{-\tau})\exp\left[-k\, e^{-\tau}\delta\omega\right] = e^{-\tau/\epsilon}\int_{\eta_0}^{\infty} d\eta\, \eta^{-\frac{1}{\epsilon}-1}\tilde{g}_0(\eta)\, e^{-\eta\delta\omega}.$$

This clearly is of the same form as the anomalous contribution in our previous result (50). The (unknown) function $\hat{\beta}_0(\zeta)$ is given by the integral involving the (unknown) function $\tilde{g}_0(\eta)$. By construction the result (76) is valid for large k and large τ and therefore picks up the structure of the singularities for $\tau \gg 1$. We conclude that the anomalous contribution $e^{-\tau/\epsilon}\hat{\beta}_0(\zeta)$ is due to the singularities which approach $\omega = -1$, as claimed above.

We finally note that the leading singularity $\sim(1-\omega)^{1/\epsilon+\lambda}$ of the eigenfunction $\beta_\lambda(\omega)$ implies that the Taylor coefficients of $e^{\lambda\tau}\beta_\lambda(\omega)$ for large k behave as

$$b_k(\tau) \sim (-1)^k k^{-\frac{1}{\epsilon}-1}\left(\frac{e^{\tau}}{k}\right)^{\lambda} C_1\left(1+\mathcal{O}\left(\frac{1}{k}\right)\right),$$

where C_1 is some constant. We thus recover the form (76) with $\tilde{g}_0(\eta) = \eta^{-\lambda}$.

3.6. Rigorous analysis of the limit $\tau \to \infty$

In the previous subsection we have argued that $\beta(\omega,\tau)$ for $\tau \to \infty$ tends to a function $\beta_\infty(\omega)$ that is analytic in any compact subset $\mathcal{K}$ of $\overline{\mathcal{U}}_\omega \setminus \{-1\}$. Furthermore, the eigenvalue analysis [19] as well as the results of Sections 3.2–3.4 suggest that within the linearized theory a perturbation for $\tau \to \infty$ only leads to a constant shift of the circle. Assuming the existence of $\beta_\infty(\omega)$, this can be proved rigorously.

We start from Eq. (13): $\mathcal{L}_\epsilon\beta = 0$, rewritten as

$$\left[\left(1-T^2\right)\partial_T - \left(1-\omega^2\right)\partial_\omega\right](1+\epsilon+\epsilon\omega\partial_\omega)\,\beta\,(\omega,\tau(T)) = (1-\epsilon)\left(1+\omega^2\right)\partial_\omega\beta\,(\omega,\tau(T)), \tag{77}$$

where $T = \tanh\tau/2$, (Eq. (18)), and we introduce the function

$$G(\omega,T) = (1+\epsilon+\epsilon\omega\partial_\omega)\,\beta\,(\omega,\tau(T)). \tag{78}$$

In terms of $G(\omega,T)$ the solution $\beta(\omega,\tau)$ regular at $\omega = 0$ is given by

$$\beta(\omega,\tau) = \frac{1}{\epsilon}\omega^{-1/\epsilon-1}\int_0^{\omega} \omega'^{1/\epsilon} G(\omega', T(\tau))d\omega' \tag{79}$$

which generalizes Eq. (16) to $\epsilon \neq 1$. We now write Eq. (77) as

$$\left[\left(1-T^2\right)\partial_T - \left(1-\omega^2\right)\partial_\omega\right]G(\omega,T) = H\,(\omega,T), \tag{80}$$

where

$$H(\omega,T) = \frac{1-\epsilon}{\epsilon}\frac{1+\omega^2}{\omega}\left[G(\omega,T) - \frac{1+\epsilon}{\epsilon}\int_0^1 x^{1/\epsilon}G(x\omega,T)dx\right]. \tag{81}$$

Noting that $G(\omega,T) \equiv \zeta = (\omega+T)/(1+\omega T)$ solves Eq. (80) for $H \equiv 0$ it is easily found that (80) is equivalent to the integral equation

$$G(\omega,T) = G(0,\zeta) - \int_0^{\omega}\frac{1}{1-\omega'^2}H\left(\omega', \frac{\zeta-\omega'}{1-\omega'\zeta}\right)d\omega'. \tag{82}$$

We now define

$$\Delta(\omega,T) = G(\omega,T) - G(0,T). \tag{83}$$

Eq. (82) yields

$$\Delta(\omega,T) = G(0,\zeta) - G(0,T) - \frac{1-\epsilon}{\epsilon}\int_0^{\omega}\frac{1}{\omega'}\frac{1+\omega'^2}{1-\omega'^2}\left[\Delta\left(\omega', \frac{\zeta-\omega'}{1-\omega'\zeta}\right) - \frac{1+\epsilon}{\epsilon}\int_0^1 x^{1/\epsilon}\Delta\left(x\omega', \frac{\zeta-\omega'}{1-\omega'\zeta}\right)dx\right]d\omega', \tag{84}$$

where we have written out H explicitly. In view of the results of Section 3.5 we now assume that $\lim_{T\to 1} G(\omega,T)$ exists for $\omega \in \mathcal{K}$. We further note that for $T \to 1$ and $\omega \neq -1$, both ζ and $(\zeta-\omega')/(1-\omega'\zeta)$ tend to 1. Eq. (84) reduces to the homogeneous integral equation

$$\Delta(\omega,1) = -\frac{1-\epsilon}{\epsilon}\int_0^{\omega}\frac{1}{\omega'}\frac{1+\omega'^2}{1-\omega'^2}\left[\Delta(\omega',1) - \frac{1+\epsilon}{\epsilon}\int_0^1 x^{1/\epsilon}\Delta\left(x\omega',1\right)dx\right]d\omega'. \tag{85}$$

It is easily checked that for all $\epsilon > 0$ the only solution of (85) analytic in a neighborhood of $\omega = 0$ is the trivial one:

$$\Delta(\omega,1) \equiv 0. \tag{86}$$

To see this, we assume that the Taylor expansion of $\Delta(\omega,1)$ starts with a lowest order term $a_k\omega^k$, $k \geq 1$, $a_k \neq 0$. Eq. (85) yields $a_k = 0$, contradicting our assumption.

We thus have shown that provided $G(\omega,1)$ exists and is analytic for $\omega \in \mathcal{K}$, the only solution to our problem is

$$G(\omega,1) \equiv G(0,1), \tag{87}$$

implying

$$\beta_\infty(\omega) = \frac{G(0,1)}{1+\epsilon}, \tag{88}$$

which for $\epsilon = 1$ reduces to Eq. (20).

3.7. Numerical illustration

In this section, we show numerical results of the linear evolution. We approximately solve the PDE (14) by truncating the series expansion (64),

$$\beta = \sum_{k=0}^{\infty} b_k\omega^k,$$

at $k = N$. The ODE system for $b_k(\tau)$ has been given in Eq. (65)

$$2\partial_\tau b_0 = \frac{2+\epsilon}{1+\epsilon}b_1,$$
$$2\partial_\tau b_k = \frac{k+1}{1+\epsilon+\epsilon k}\times\left[(2+\epsilon+\epsilon k)b_{k+1} - \epsilon(k-1)b_{k-1}\right] \quad \text{for } k \geq 1.$$

With the $b_k(0)$ given by the initial condition, the $b_k(\tau)$ can be determined recursively by the Runge–Kutta time stepping method. We choose the cut-off $N = 2000$ in the simulation. Adaptive time steps are chosen which ensure that the difference between 4-th order and 5-th order Runge–Kutta methods is within 10^{-15}. In the following we present results for

$$\delta\beta(\omega,\tau) = \beta(\omega,\tau) - \beta(0,\tau). \tag{89}$$

The subtraction eliminates the overall shift of the evolving body.

We first present results typical for a delocalized initial condition, choosing

$$\beta(\omega,0) = \omega^5. \tag{90}$$

Fig. 5 shows the evolution of $\mathrm{Re}[\omega\delta\beta(\omega,\tau)]$, $\omega = e^{i\alpha}$, with $\epsilon = 1/10$ or $\epsilon = 1/2$, respectively. In physical space, $\mathrm{Re}[\omega\delta\beta]$ is the component of the perturbation normal to the unperturbed but

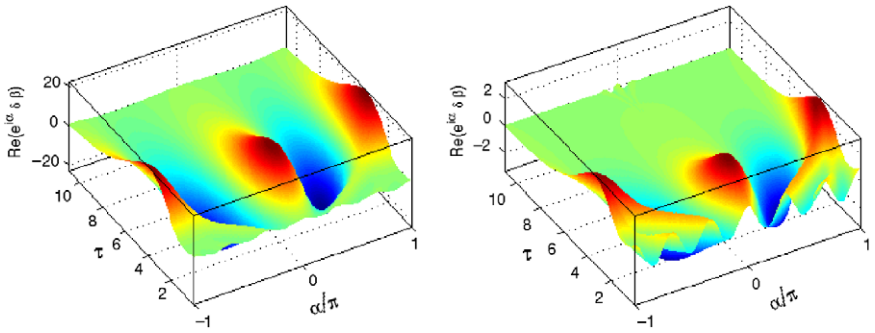

(a) $\epsilon = 1/10$. (b) $\epsilon = 1/2$.

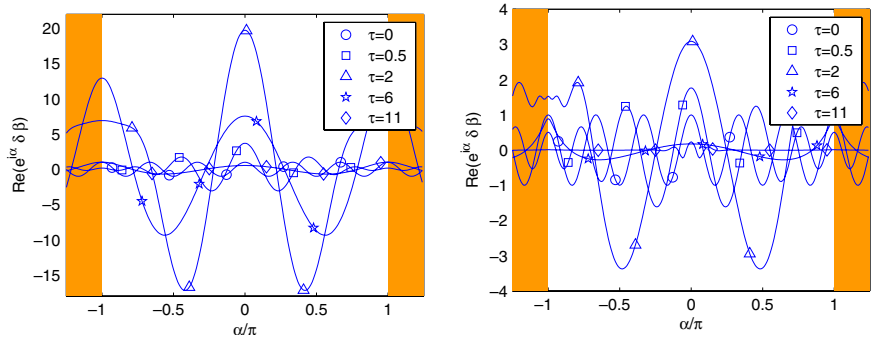

(c) Times 0, 0.5, 2, 6 for $\epsilon = 1/10$. (d) Same time steps for $\epsilon = 1/2$.

Fig. 5. Evolution of $\mathrm{Re}[\omega\delta\beta(\omega,\tau)]$ for $\omega = e^{i\alpha}$ for the initial condition (90). (a) Overview plot for $\epsilon = 1/10$ and times $0 \le \tau \le 11$. (b) The same for $\epsilon = 1/2$ and times $0 \le \tau \le 11$. (c) Detailed data for time steps 0, 0.5, 2, 6, 11 for $\epsilon = 1/10$; the angle is normalized as α/π; orange areas are overlap regions plotted to make the structure at the back visible. (d) The same for $\epsilon = 1/2$.

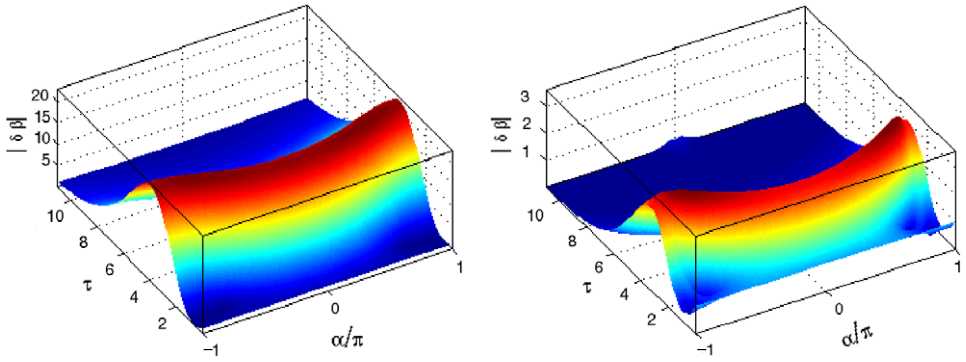

(a) $\epsilon = 1/10$. (b) $\epsilon = 1/2$.

Fig. 6. Evolution of $|\delta\beta(\omega,\tau)|$ for the initial condition (90) with (a) $\epsilon = 1/10$ and (b) $\epsilon = 1/2$.

shifted circle at angle $-\alpha$. Panels (a) and (b) show that the qualitative behavior is quite similar for both values of ϵ shown. Panels (c) and (d) give a detailed view on the state for several time steps; here an extended range of α is shown, so that the behavior both at $\alpha = 0$ and $|\alpha| = \pi$ is clearly seen. For small times the perturbations increase in the front half $|\alpha| < \pi/2$ of the circle and decrease in the back half. The maximum at $\alpha = 0$ increases and broadens strongly, whereas the other perturbations are shifted towards $\alpha = \pm\pi$. At later times the perturbations decrease at the front half, while at the back a transient increase is observed which is due to the advection of the dynamically generated large amplitude of the perturbation towards $\alpha = \pi$. The results for $\epsilon = 1/10$ or $\epsilon = 1/2$ essentially differ only in two respects. First, for $\epsilon = 1/10$ the perturbation at intermediate times is amplified much more than for $\epsilon = 1/2$. Second, for $\tau = 2$ and $\epsilon = 1/2$, the remainders of individual maxima that initially are located at $\alpha \neq 0$, still can be seen near $\alpha = \pm\pi$ (this structure was very pronounced for $\epsilon = 1$ as discussed in [18]), whereas for $\epsilon = 1/10$ this structure is completely damped out and yields a broad maximum.

Fig. 6 shows $|\delta\beta|$ as a function of α and τ. It illustrates how the maximum of the absolute value of the perturbation is advected towards $\alpha = \pi$, where it decays. For $\epsilon = 1/10$ the behavior of $|\delta\beta|$ is quite smooth, whereas for $\epsilon = 1/2$ some small scale structure is observed near $\alpha = \pm\pi$.

Outside a neighborhood of $\alpha = \pi$ we expect to see asymptotically exponential relaxation: $\delta\beta \sim e^{\lambda_1\tau}$. From the results given in paper I [19] in Fig. 2, we expect $\lambda_1 \approx -0.546$ for $\epsilon = 1/10$, and $\lambda_1 \approx -0.905$ for $\epsilon = 1/2$, respectively. These predictions are tested in Fig. 7. Since the maximum of $|\delta\beta|$ advects along the circle, we plot $\ln|\delta\beta_{\max}(\tau)|$ as a function of τ, where

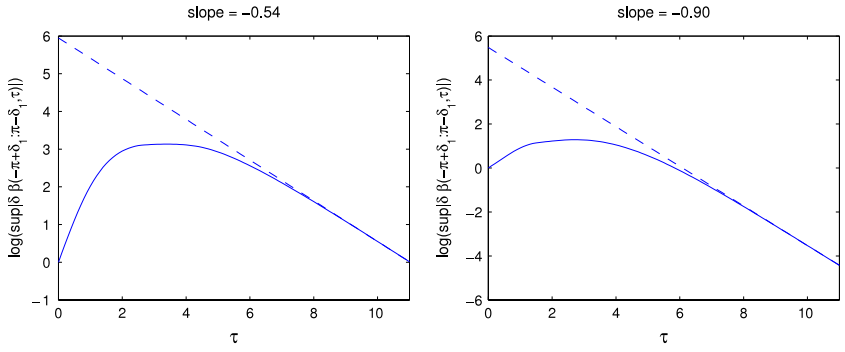

(a) $\epsilon = 1/10$. (b) $\epsilon = 1/2$.

Fig. 7. $\log \sup_{\alpha\in[-\pi+\delta_1,\pi-\delta_1]} |\delta\beta(\alpha,\tau)|$, $\delta_1 = \pi/8$ as a function of τ for the data presented in Fig. 6. (a) $\epsilon = 1/10$, the line has slope $\lambda_1(1/10) = -0.54$. (b) $\epsilon = 1/2$, the line has slope $\lambda_1(1/2) = -0.90$.

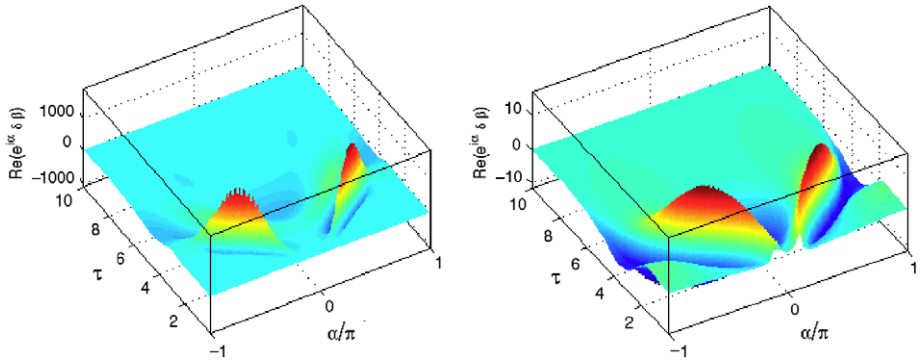

(a) $\epsilon = 1/10$. (b) $\epsilon = 1/2$.

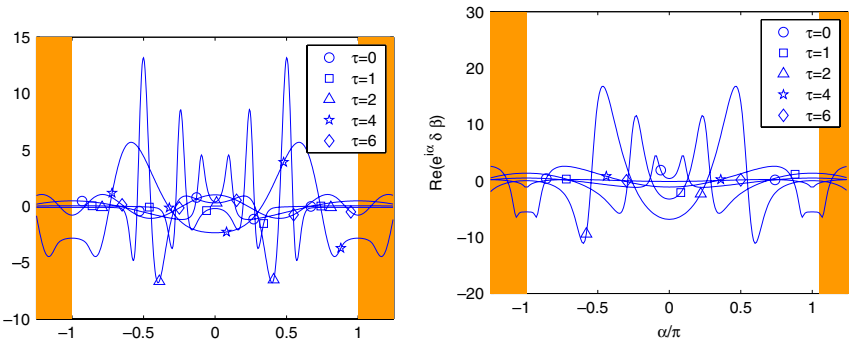

(c) $\epsilon = 1/10$. (d) $\epsilon = 1/2$.

Fig. 8. Evolution of $\mathrm{Re}[\omega\delta\beta(\omega,\tau)]$ for the initial condition (91) with $\gamma = 1.1\,\mathrm{e}^{-\mathrm{i}\pi/10}$ for $\epsilon = 1/10$ and $\epsilon = 1/2$. In panel (c), $\mathrm{Re}(\omega\delta\beta)$ is scaled by factors $\alpha_0(\tau)$, where $\alpha_0(0) = 1, \alpha_0(1) = 0.03, \alpha_0(2) = 0.007, \alpha_0(4) = 0.025, \alpha_0(6) = 0.05$.

$$|\delta\beta_{\max}(\tau)| = \sup_{\alpha\epsilon[\pi+\delta_1,\pi-\delta_1]} |\delta\beta(\mathrm{e}^{\mathrm{i}\alpha},\tau)|.$$

We choose $\delta_1 = \pi/8$. For smaller values of δ_1 it needs larger values of τ to reach the asymptotic behavior. We fit the curve for data at $10 \le \tau \le 11$. As Fig. 7 illustrates, the expected asymptotic behavior is observed.

We now consider a more localized initial condition:

$$\beta(\omega,0) = \frac{1}{2}\left(\frac{\gamma}{\gamma-\omega} + \frac{\gamma^*}{\gamma^*-\omega}\right) = \frac{1}{2}\sum_{j=0}^{\infty}\left[\left(\frac{\omega}{\gamma}\right)^j + \left(\frac{\omega}{\gamma^*}\right)^j\right]. \tag{91}$$

With the choice $\gamma = 1.1\mathrm{e}^{\mathrm{i}\pi/10}$ it shows two fairly sharp peaks centered symmetrically close to $\alpha = 0$. Similar to Fig. 5, Fig. 8 shows $\mathrm{Re}(\omega\delta\beta(\omega,\tau))$ for $\epsilon = 1/10$ and $\epsilon = 1/2$. For $\epsilon = 1/10$ we rescaled the amplitude in panel (c) by a time dependent factor $a_0(\tau)$ in order to show all curves in the same plot. Panels (a) and (b) show that the time dependent shift of the structure is essentially independent of ϵ, implying that advection is determined by the automorphism $\zeta = \zeta(\omega, T(\tau))$. Panels (c) and (d) illustrate that also the detailed structure at given time τ is fairly independent of ϵ, but for $\epsilon = 1/10$ the amplitude at intermediate times is enhanced much more than for $\epsilon = 1/2$ (cf. the rescaling factors $a_0(\tau)$ given in the figure caption). Fig. 9 shows $|\delta\beta|$ as a function of α and τ, similarly to Fig. 6. Again the advection of the maximum towards $\alpha = \pi$, its increase as long as it is in the front half, and its final decay in the back half are clearly seen.

In summary, all numerical results presented here and in previous subsections support our analysis.

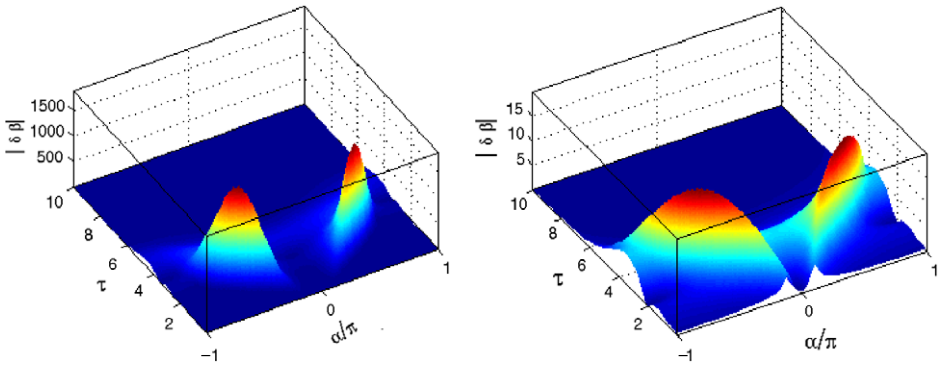

(a) $\epsilon = 1/10$. (b) $\epsilon = 1/2$.

Fig. 9. The same evolution as in Fig. 8; now $|\delta\beta(\alpha, \tau)|$ is plotted as a function of α and τ. Left column: $\epsilon = 1/10$, right column: $\epsilon = 1/2$. Note the large difference in the scale of $|\delta\beta|$, reflecting the strong ϵ dependence of the amplitude.

4. Nonlinear evolution

In Section 3 we discussed the solution of the linearized evolution equation. Here we seek to determine the effect of the nonlinearity. In Section 4.1 we consider small perturbations of the circle. Section 4.2 presents examples of the evolution of more general initial shapes.

To calculate the nonlinear evolution in a large range of time is difficult. Using a Fourier representation of the interface it needs wavenumbers of order $e^{\tau} \gg 1$ for large τ to resolve the collapsing region near $\omega = -1$. Modes of large wavenumber can also be expected to play an important role at the front part of the bubble. Approximating a small region near $\omega = +1$ as planar, we may invoke well known results [28,29,33] on the instability of a planar interface: in linear approximation the amplitude of a Fourier mode of wavenumber k increases like $e^{s(k)\tau}$, where

$$s(k) = \frac{k}{1 + \epsilon k}.$$

Thus with the present regularization all Fourier modes are unstable, whereas with curvature regularization only a finite unstable band exists. The strong increase of a perturbation localized near $\omega = +1$, as discussed in Section 3.3, can be considered to result from this instability of modes $k \gg 1/\epsilon$. Nonetheless, despite stringent demands on resolution and time steps, we believe that the results presented here exemplify the nonlinear effects. The numerical methods used to solve the nonlinear equations (9) and (10) are summarized in the Appendix. We use a Fourier representation with cutoff $k_{\max} = N$, and we solve the resulting system of ordinary differential equations with a 4th order Runge–Kutta method with time step Δt. (N and Δt are given in the figure captions.) The numerics abruptly breaks down at some time $t_{\max}(\epsilon)$. The time range shown in the figures therefore depends both on ϵ and on the initial condition.

4.1. Small perturbations of the circle

We here consider perturbations $\eta\beta(\omega, 0)$ of the circle, with $\eta \ll 1$. In order to compare with the linear evolution we define the nonlinear counterpart to $\delta\beta(\omega, \tau) = \beta(\omega, \tau) - \beta(0, \tau)$ as

$$\delta\beta_{nl}(\omega, \tau) = \frac{\hat{f}(\omega, t) - \hat{f}(0, t)}{\eta}, \tag{92}$$

where $t = \frac{1+\epsilon}{2}\tau$, Eq. (15), and $\hat{f}(\omega, t)$ is defined in Eq. (6). For $\eta \to 0$, $\delta\beta_{nl}$ reduces to $\delta\beta$.

We first consider the delocalized initial condition (90): $\hat{f}(\omega, 0) = \eta\omega^5$. Even for very small η it is not obvious a priori that the nonlinearity is unimportant. As recalled above, perturbations at the front may increase dramatically, and the collapsing region at the back, where an eigenmode expansion is bound to fail, also might be quite sensitive to nonlinear effects. We therefore in Fig. 10 show $\delta\beta_{nl}(+1, \tau)$ and $\delta\beta_{nl}(-1, \tau)$ for $\epsilon = \frac{1}{10}$ or $\frac{1}{2}$ and several values of η. It is seen that for very small values of η the nonlinear theory essentially reproduces the results of the linear approximation. Deviations outside some initial time range become visible for $\eta \geq 10^{-4}$, $\left(\epsilon = \frac{1}{10}\right)$, or $\eta \geq 10^{-3}$, $\left(\epsilon = \frac{1}{2}\right)$, respectively, but even then the shape of the curves is similar to the linear approximation. This suggests that also in the forward and backward regions the nonlinearity for small perturbations does not qualitatively change the results of the linear approximation.

The results shown in Fig. 11 support this conclusion. We here plot $\mathrm{Re}(e^{i\alpha}\delta\beta_{nl}(e^{i\alpha}, \tau))$ as a function of α/π, for values of τ where a deviation from the linear approximation is visible. We observe that the nonlinearity essentially influences the amplitude but not the shift of the perturbation. The overall structure is most similar to the linear approximation.

Such results are also found for other delocalized perturbations of type $\eta\omega^n$. Also more localized perturbations behave similar. For the initial condition (91), $\beta(\omega, 0) = \frac{1}{2}\frac{\gamma}{\gamma-\omega} + \frac{1}{2}\frac{\gamma^*}{\gamma^*-\omega}$ this is illustrated in Fig. 12. We again observe that the nonlinearity essentially influences only the amplitude of the perturbation, but leaves the qualitative structure almost unchanged. All these results suggest that the circle is the asymptotic attractor for weak perturbations.

For larger initial perturbations it is unlikely that the circle is recovered asymptotically. Rather we may observe branching. This is illustrated in Fig. 13 with the initial condition $\beta(\omega, 0) = -0.03\omega^5$. Panel (a) shows snapshots of the interface in physical space $z = x + iy = f(\omega, t)$, with $\epsilon = \frac{1}{10}$, as resulting from the nonlinear evolution. For comparison panel (b) shows the linearized evolution, and panel (c) shows the result of the unregularized model $\epsilon = 0$. Snapshots are taken at times $t = 0.05n$, where $n = 0, 1, \ldots, 12$ in panels (a) and (b), and $n = 0, 1, \ldots, 5$ in panel (c). Clearly the cusps that in the unregularized model occur for $t \approx 0.25$ are suppressed for $\epsilon = \frac{1}{10}$ both according to the linear and to the nonlinear evolution. A qualitative effect of the nonlinearity is observed for $t > 0.1$. Whereas the linear approximation develops shoulders connected by some flat part of the interface, the nonlinear evolution results in two branches separated by a valley. Since the bottom of the valley moves slower than the tips of the branches, the valley is likely to evolve into a deep fjord.

To close this subsection we briefly consider the range of validity of the linear approximation. As is evident from Fig. 10, for a given initial condition this range strongly depends on ϵ. The results of Section 3.3 suggest that it might decrease exponentially:

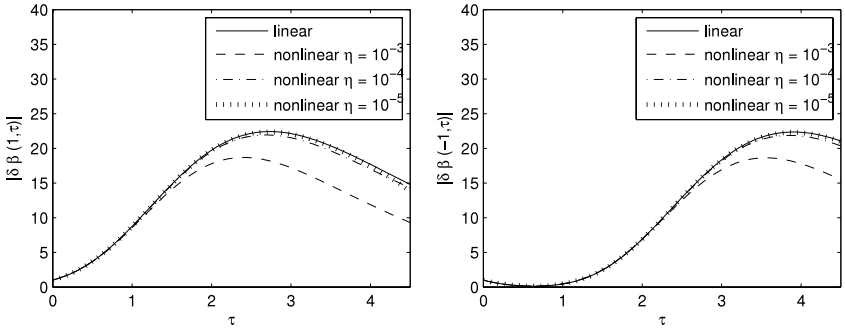

(a) $\epsilon = 1/10, \omega = 1$. (b) $\epsilon = 1/10, \omega = -1$.

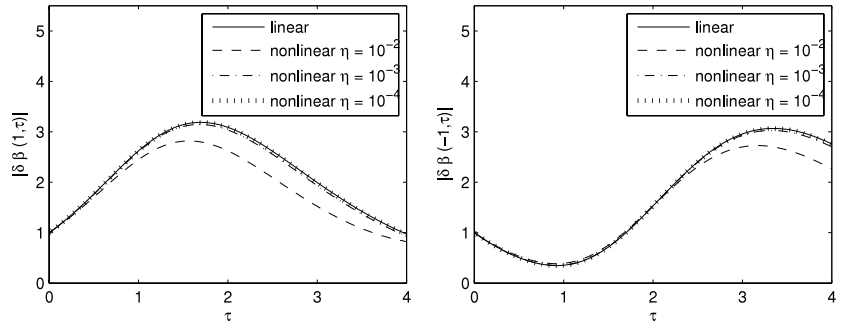

(c) $\epsilon = 1/2, \omega = 1$. (d) $\epsilon = 1/2, \omega = -1$.

Fig. 10. Initial condition: $\beta_{nl}(\omega, 0) = \omega^5$, plotted are $\delta\beta(1, \tau)$ and $\delta\beta(-1, \tau)$ as a function of τ for $\epsilon = 1/10$ and $\epsilon = 1/2$ for different η ($N = 256$, $\Delta t = 0.001$).

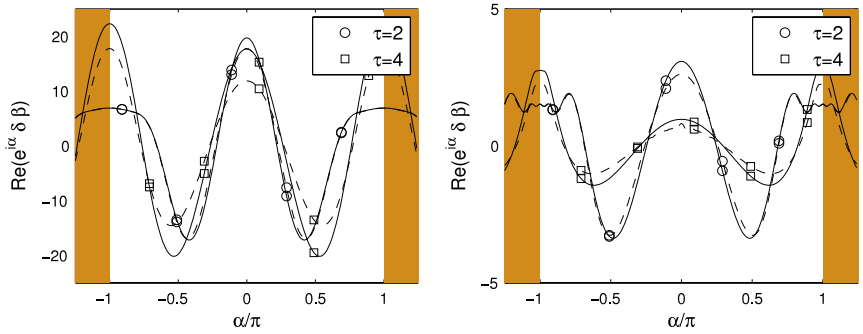

(a) $\epsilon = 1/10, \eta = 10^{-3}$. (b) $\epsilon = 1/2, \eta = 10^{-2}$.

Fig. 11. Evolution of $\mathrm{Re}[\omega\delta\beta(\omega, \tau)]$ for $\omega = e^{i\alpha}$ for the initial condition (90) for $\epsilon = 1/10$ and $\epsilon = 1/2$ at different τ ($N = 256$, $\Delta t = 0.001$). The solid lines show the linear evolution and the dashed lines the nonlinear evolution for $\eta = 10^{-3}$ in (a) or 10^{-2} in (b).

$\eta < \text{const}\ e^{-\text{const}/\epsilon}$, where the constants might depend on the initial condition. To test this hypothesis, we compared for the initial condition $\beta(\omega, 0) = \eta\omega^{10}$ the linearized and the nonlinear evolution for values $\eta = 0.001 \cdot 2^{-n}, n = 0, 1, \ldots, 4$ and ϵ in the range $0.12 \le \epsilon \le 0.24$. We specifically calculated the absolute value of the difference $\partial_\omega\beta_{nl} - \partial_\omega\beta$ in forward direction $\omega = 1$. We choose the derivative since it prominently shows up in the nonlinear equations (9) and (10). The results for $\epsilon = 0.2$ are shown in Fig. 14(a). We observe that after some initial rise this difference saturates at some η-dependent plateau, where the plateau value strongly increases with η. Eventually it decreases again, in agreement with the expectation that for the small perturbations η, the circle is the asymptotic attractor. Interpolating among the plateau values we now for each ϵ determined a value $\eta^*(\epsilon)$ where the plateau value equals 0.02 at $\tau = 4$. Fig. 14(b) shows $\ln \eta^*$ as a function of $1/\epsilon$. As expected, it shows an essentially linear decrease. This supports the hypothesis that the range of validity of the linear approximation, and presumably also the basin of attraction of the circle, decrease exponentially with increasing $1/\epsilon$.

4.2. Examples of the evolution of general shapes

For general initial conditions the time evolution may lead to a breakdown of the model by two different mechanisms. First, a global breakdown occurs at time t_c where the mapping loses the property of being one-to-one: $f(e^{i\alpha_1}, t_c) = f(e^{i\alpha_2}, t_c)$ for some $\alpha_1 \neq \alpha_2$. Clearly for $t > t_c$ the model becomes invalid. Physically we might suspect that the bubble splits into two disjoint parts. Second, the model can break down locally if a zero of $\partial_\omega f(\omega, t)$ reaches the unit circle, which results in a cusp of the interface. It is well known that this is a common mechanism for breakdown in the unregularized model, ($\epsilon = 0$).

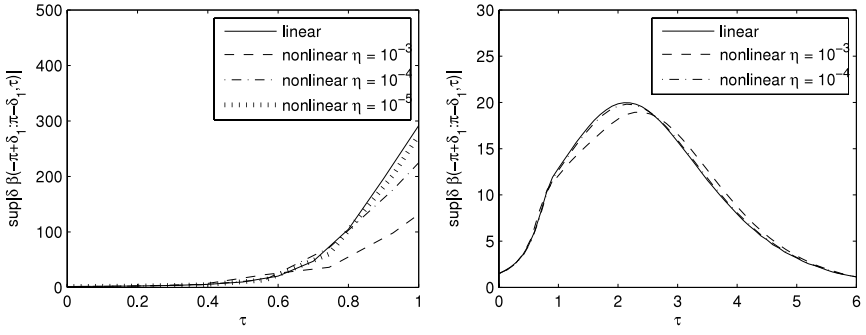

(a) $\epsilon = 1/10$. (b) $\epsilon = 1/2$.

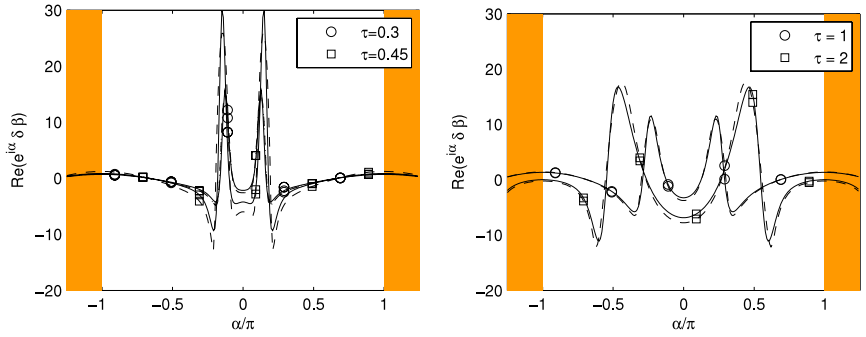

(c) $\epsilon = 1/10$, $\eta = 10^{-3}$. (d) $\epsilon = 1/2$, $\eta = 10^{-3}$.

Fig. 12. Initial condition: $\beta(\omega, 0) = \frac{1}{2}\frac{\gamma}{\gamma-\omega} + \frac{1}{2}\frac{\gamma^*}{\gamma^*-\omega}$. Plotted are $\sup_{\alpha\in[-\pi+\delta_1,\pi-\delta_1]} |\delta\beta(\alpha, \tau)|$, $\delta_1 = \pi/8$ as a function of τ for (a) $\epsilon = 1/10$ and (b) $\epsilon = 1/2$ for different η as indicated in the panels. Evolution of $\mathrm{Re}[\omega\delta\beta(\omega, \tau)]$ for $\omega = e^{i\alpha}$ for (c) $\epsilon = 1/10$ and (d) $\epsilon = 1/2$ at different τ ($N = 256$, $\Delta t = 0.001$). The solid lines again show the linear evolution and the dashed lines the nonlinear evolution for $\eta = 10^{-3}$.

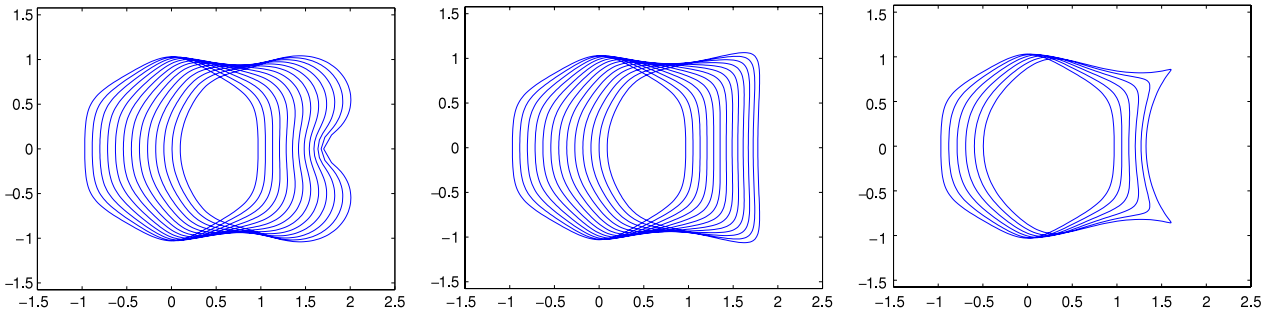

(a) $\epsilon = 1/10$, nonlinear. (b) $\epsilon = 1/10$, linear. (c) $\epsilon = 0$, nonlinear.

Fig. 13. Initial condition: $\beta(\omega, 0) = -0.03\omega^5$. (a) and (b) show the nonlinear and the linear evolution respectively for $\epsilon = 1/10$. (c) shows the nonlinear evolution for $\epsilon = 0$. ($N = 512$, $\Delta t = 0.00025$.)

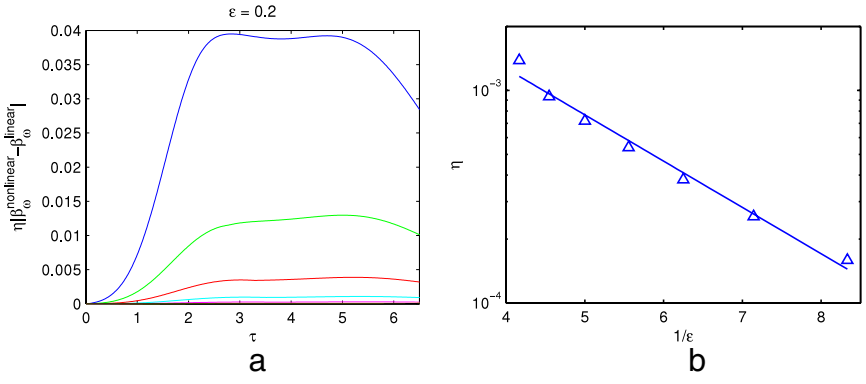

Fig. 14. (a) $\eta|\partial_\omega\beta_{nl} - \partial_\omega\beta|$ as a function of τ for $\eta = 0.001 \cdot 2^{-n}$, $n = 0, 1, \ldots, 4$ ($N = 256$, $\Delta t = 0.001$). (b) $\ln(\eta)$ as a linear function of $1/\epsilon$. The fitting curve is $\ln(\eta) = -0.5/\epsilon - 4.66$.

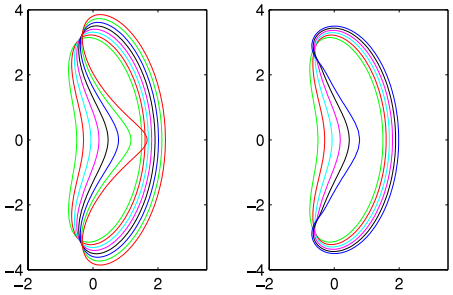

(a) $\epsilon = 0, n = 0 : 7.$ (b) $\epsilon = 0.01, n = 0 : 5.$

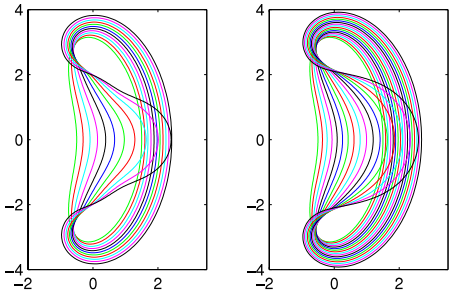

(c) $\epsilon = 0.1, n = 0 : 10.$ (d) $\epsilon = 1, n = 0 : 16.$

Fig. 15. $f(\omega, 0) = \frac{1}{\omega} - 2\omega + 0.5\omega^2$ ($N = 512$, $\Delta t = 0.0005$). The solutions are shown at $t = 0.2n$.

Global breakdown has been observed with curvature regularization (see, e.g., [34]), and is also observed in our model. Figs. 15 and 16 show examples, where each figure shows the evolution of a given initial condition for several values of ϵ. For $\epsilon = 0$ cusps do form, as is particularly obvious in Fig. 16(a). The regularization $\epsilon > 0$ suppresses the cusps, but does not change the tendency to split into two parts.

Whether local breakdown by cusp formation can occur in the regularized model is a more difficult question. We recall that the neighborhood of $\omega = -1$ shows a special dynamics. The linearized evolution of the interface can lead to a very complicated shape near $\omega = -1$ since with increasing time singularities of $f(\omega, 0)$ are gathered in this neighborhood. According to Section 3.4 these singularities for $\epsilon \geq 1/2$ dominate the local structure of the interface. We also note that for $\epsilon = \infty$ even the linearized evolution is singular at $\omega = -1$, where it produces a spike. It thus is conceivable that the nonlinear evolution yields a cusp or some other type of singularity at $\omega = -1$.

We studied this problem with the initial condition $f(\omega, 0) = 1/\omega - 0.1\omega^2$. The results of the nonlinear evolution are shown in Fig. 17. Clearly the cusps forming for $\epsilon = 0$ in the front part are suppressed for $\epsilon > 0$. We further observe that for $\epsilon = 1/100$ or $1/10$, the curvature near $\omega = -1$ decreases, whereas it increases for $\epsilon = 1$. This suggests that for $\epsilon = 1$ a cusp may be formed.

5. Summary and conclusion

Consistent with the eigenvalue analysis presented in [19], the results of the present paper strongly suggest that a uniformly translating circle is a linearly stable solution of a Laplacian interface model regularized by a kinetic undercooling boundary condition. Furthermore, numerical results of the full nonlinear evolution indicate that the circle has a finite basin of attraction in a space of analytic functions. An important feature of the stabilizing mechanism is the advection of perturbations towards the back of the circle. Except for a small region at the back that asymptotically contracts to a point, the final relaxation to the circle is exponential. With decreasing regularization parameter $\epsilon > 0$ the anomalous behavior at the back is suppressed. However, perturbations increase as long as they are in the front half of the circle, and this effect is strongly enhanced by lowering ϵ. Since larger perturbations may lead to branching, this indicates that the basin of attraction of the circle shrinks exponentially with decreasing ϵ.

The interface model considered here is a reduced form of a PDE-model describing the streamer stage of electric breakdown in the simplest physically relevant situation. It ignores the physics inside the streamer and the internal structure of the screening layer; the layer is approximated by the interface together with the boundary condition (3) which introduces the regularization. Numerical solutions of the PDE-model indicate that these approximations for sufficiently strong externally applied fields are justified in the dynamically active front part of the streamer. The back of the streamer is not represented adequately by the interface model. However, the evolution of the streamer and in particular stability or instability against branching is determined by the active head region, which corresponds to the front half of the circle in our analysis. Indeed, numerical solutions of the PDE-model in two dimensions show a behavior quite similar to the evolution of the front half of weakly disturbed circles in the interface model. After reaching the streamer stage the streamer head is of nearly circular shape and moves with constant velocity. It slowly flattens at the tip and branches. Compared to the results of the interface model as illustrated in Fig. 13, the main difference is a slow increase of

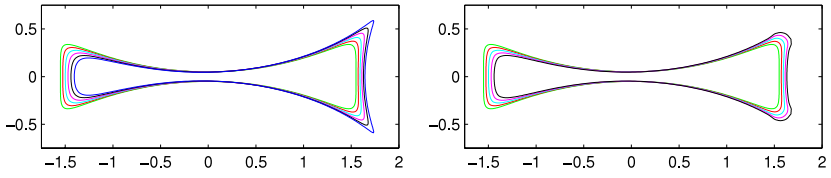

(a) $\epsilon = 0, n = 0 : 5.$ (b) $\epsilon = 0.01, n = 0 : 4.$

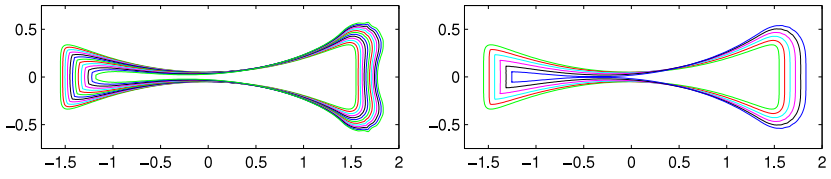

(c) $\epsilon = 0.1, n = 0 : 10.$ (d) $\epsilon = 1, n = 0 : 5.$

Fig. 16. $f(\omega, 0) = \frac{1}{\omega} + 0.75\omega - 0.2\omega^3$ ($N = 512$, $\Delta t = 0.0005$). The solutions are shown at $t = 0.01n$ for (a), (b), (c) and at $t = 0.05n$ for (d).

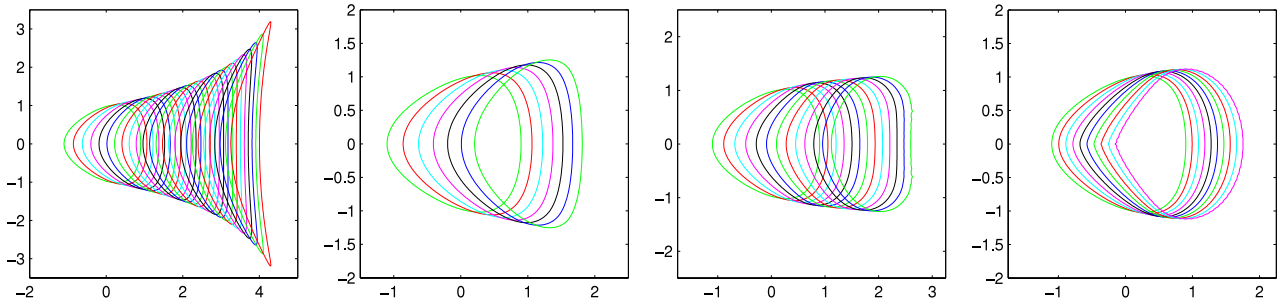

(a) $\epsilon = 0, n = 0:25$. (b) $\epsilon = 0.01, n = 0:6$. (c) $\epsilon = 0.1, n = 0:12$. (d) $\epsilon = 1, n = 0:9$.

Fig. 17. Ice-cone: $f(\omega, 0) = \frac{1}{\omega} - 0.1\omega^2$ ($N = 512$, $\Delta t = 0.0005$). The solutions are shown at $t = 0.1n$.

the head radius due to weak currents flowing into the head from the interior of the streamer.

In summary, we believe that our results not only are of some interest in the context of interface models but also shed some light on the problem of streamer branching.

Acknowledgements

ST was supported by US National Science Foundation DMS-0807266 and acknowledges hospitality at CWI Amsterdam. FB acknowledges a grant of The Netherlands' Organization for Scientific Research NWO within the FOM/EW-program "Dynamics of Patterns". CYK was partially supported by the National Science Foundation grant DMS-0811003 and an Alfred P. Sloan Fellowship.

Appendix. Numerical calculation of the nonlinear evolution

As explained in Section 2 the shape of the interface is given by

$$z = x + \mathrm{i}y = f\left(\mathrm{e}^{\mathrm{i}\alpha}, t\right), \quad -\pi < \alpha \leq \pi.$$

We restrict ourselves to interfaces symmetric with respect to the real axis, so that

$$f^*\left(\mathrm{e}^{\mathrm{i}\alpha}, t\right) = f\left(\mathrm{e}^{-\mathrm{i}\alpha}, t\right),$$

with the corresponding equation holding for the potential $\Phi(\mathrm{e}^{\mathrm{i}\alpha}, t)$. We use the Fourier representation

$$f = \sum_{k=-1}^{\infty} a_k(t)\mathrm{e}^{\mathrm{i}k\alpha}, \tag{93}$$

$$\Phi = \sum_{k=-1}^{\infty} c_k(t)\mathrm{e}^{\mathrm{i}k\alpha}, \tag{94}$$

with a cutoff at high wavenumber $k = N$. Due to the symmetry, $a_k(t)$ and $c_k(t)$ are real, and the boundary condition at infinity (5) enforces $c_{-1}(t) \equiv a_{-1}(t)$.

For a given shape of the interface the potential is determined by Eq. (10):

$$|\partial_\alpha f\left(\mathrm{e}^{\mathrm{i}\alpha}, t\right)| \operatorname{Re}\left[\Phi\left(\mathrm{e}^{\mathrm{i}\alpha}, t\right)\right] = \epsilon \operatorname{Re}\left[\mathrm{i}\partial_\alpha \Phi\left(\mathrm{e}^{\mathrm{i}\alpha}, t\right)\right]. \tag{95}$$

We represent $|\partial_\alpha f|$ as

$$|\partial_\alpha f| = \sum_{k=-\infty}^{\infty} d_k(t)\mathrm{e}^{\mathrm{i}k\alpha}, \tag{96}$$

where the symmetry enforces $d_k = d_{-k} \in \mathbb{R}$. For a given f in Fourier representation (93),

$$\partial_\alpha f = \sum_{k=-1}^{\infty} \mathrm{i}k a_k(t)\mathrm{e}^{\mathrm{i}k\alpha}. \tag{97}$$

The nonlinear term $|\partial_\alpha f|$ is computed via the standard pseudo-spectral approach, i.e. $|\partial_\alpha f|$ is obtained in the physical domain via inverse Fourier transform of Fourier coefficients in (97) and taking the absolute value and then d_k is determined by the Fourier transform of $|\partial_\alpha f|$. Substituting Eqs. (94) and (96) into Eq. (95), we find a system of linear equations for $c_k, k \geq 0$, which can be written as

$$\sum_{k=0}^{\infty}(d_{m-k} + d_{m+k} + \epsilon m\delta_{m,k})c_k = (\epsilon\delta_{m,1} - d_{m+1} - d_{m-1})a_{-1}, \quad m \geq 0. \tag{98}$$

Here $\delta_{m,k}$ denotes Kronnecker's symbol, and we used the identity $c_{-1} \equiv a_{-1}$. We solve these equations with a cutoff k, $m \leq N$. Note that d_k is needed up to $k = 2N$.

The evolution of the interface is determined by Eq. (9), which can be written as

$$\operatorname{Re}\left[\frac{\partial_t f}{\omega\partial_\omega f}\right] = \frac{\operatorname{Re}\left[-\mathrm{i}\partial_\alpha \Phi\left(\mathrm{e}^{\mathrm{i}\alpha}\right)\right]}{|\partial_\alpha f|^2} = R(\alpha). \tag{99}$$

$\frac{\partial_t f}{\omega\partial_\omega f}$ is analytic for $\omega \in \mathcal{U}_\omega$ and is real for $\omega = 0$ by construction. Eq. (99) therefore implies

$$\left.\frac{\partial_t f(\omega, t)}{\omega\partial_\omega f(\omega, t)}\right|_{\omega=\mathrm{e}^{\mathrm{i}\alpha}} = \frac{1}{2\pi}\int_{-\pi}^{\pi} \frac{\mathrm{e}^{\mathrm{i}\alpha'} + \omega}{\mathrm{e}^{\mathrm{i}\alpha'} - \omega} R(\alpha')\,\mathrm{d}\alpha',$$

which for $\omega \to \mathrm{e}^{\mathrm{i}\alpha}$ reduces to

$$\left.\frac{\partial_t f}{\omega\partial_\omega f}\right|_{\omega=\mathrm{e}^{\mathrm{i}\alpha}} = R(\alpha) - \frac{\mathrm{i}}{2\pi} P\int_{-\pi}^{\pi} \cot\frac{\alpha'}{2} R(\alpha + \alpha')\,\mathrm{d}\alpha', \tag{100}$$

where P denotes the principal value. Symmetry enforces $R(\alpha) = R(-\alpha)$, so that $R(\alpha)$ can be represented as

$$R(\alpha) = \sum_{k=0}^{\infty} r_k \cos(k\alpha), \quad r_k \in \mathbb{R}, \tag{101}$$

where the r_k again are determined by the Fourier-cosine transform numerically. Substituting the expansions (93) and (101) into Eq. (100), we get

$$\frac{\mathrm{d}a_k}{\mathrm{d}t} = \sum_{n=0}^{k+1}(k - n)a_{k-n}r_n, \quad k \geq -1. \tag{102}$$

We again truncate this system of ODEs at $k = N$ and solve it via the 4-th order Runge–Kutta method (RK4) [35]. Let the initial value problem (102) be specified as follows.

$$\frac{\mathrm{d}y}{\mathrm{d}t} = f(t, y), \qquad y(t_0) = y_0, \tag{103}$$

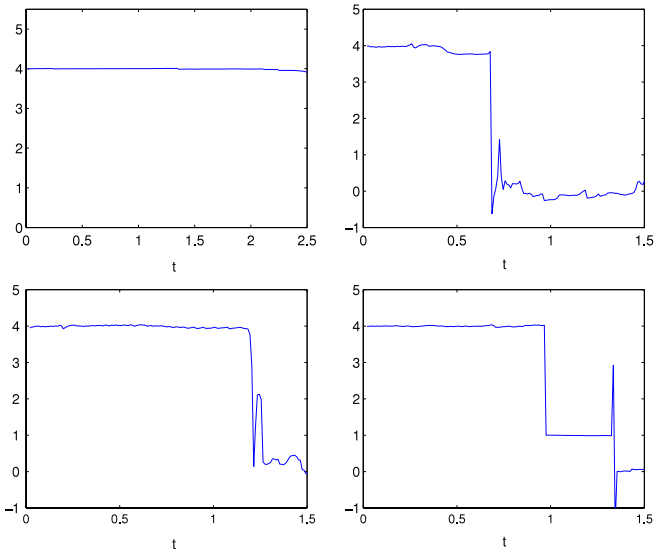

Fig. 18. Numerical estimation of the order of accuracy p (113) for the initial condition $f(\omega, 0) = \frac{1}{\omega} - 0.1\omega^2$ with (a) $\epsilon = 0$, (b) $\epsilon = 0.01$, (c) $\epsilon = 0.1$, and (d) $\epsilon = 1$ ($N = 64$).

where y denotes the vector function $(a_{-1}, a_0, a_1, \ldots, a_N)$. Then, the RK4 method for this problem is given by the following equations

$$y_{n+1} = y_n + \frac{1}{6}h(k_1 + 2k_2 + 3k_3 + k_4), \tag{104}$$

$$t_{n+1} = t_n + h, \tag{105}$$

where y_{n+1} is the RK4 approximation of $y(t_{n+1})$,

$$k_1 = f(t_n, y_n), \tag{106}$$

$$k_2 = f\left(t_n + \frac{1}{2}h, y_n + \frac{1}{2}hk_1\right), \tag{107}$$

$$k_3 = f\left(t_n + \frac{1}{2}h, y_n + \frac{1}{2}hk_2\right), \tag{108}$$

$$k_4 = f(t_n + h, y_n + hk_3), \tag{109}$$

and h is the time step. In the numerical implementation, h needs to be chosen small enough to ensure numerical stability and it is usually inversely proportional to the cut-off N. The cut-off N needs to be chosen large enough so that the interface can be smoothly represented, i.e. the Fourier coefficients decay exponentially for large k. For most of the initial conditions we used, there are only a few Fourier coefficients that are not zero. As time evolves, the number of nonzero Fourier coefficients will increase. When the high frequency mode is no longer exponentially small, the algorithm needs to be terminated or more Fourier modes need to be used. Adaptive Fourier modes are beyond the scope of this paper. Here we only use a fixed cut-off N and make sure that the high frequency modes are exponentially small at later times. In the numerical simulations, we use both double and quadruple precision to compute solutions for large enough N. To prevent the spurious growth of the high-wavenumber coefficient generated by run-off error, we filter out the coefficient which is below the chosen threshold. If the threshold is chosen to be too large, aliasing may occur. If the threshold is chosen to be too small, it cannot effectively reduce the run-off error. The reasonable choice from experience is about 1000 bigger than the run-off error. We choose the threshold to be 10^{-13} for double precision and 10^{-29} for quadruple precision. We can compare the results from both precisions to ensure the results we obtained are not spurious.

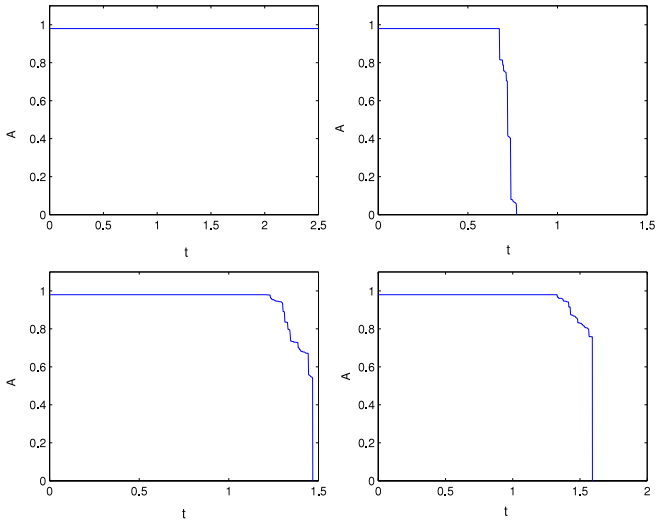

Fig. 19. Estimation of area A (114) for the initial condition $f(\omega, 0) = \frac{1}{\omega} - 0.1\omega^2$ with (a) $\epsilon = 0$, (b) $\epsilon = 0.01$, (c) $\epsilon = 0.1$, and (d) $\epsilon = 1$ ($N = 64$).

Notice that the numerical simulation needs to stop at some finite time because of singularities. When a singularity develops, the numerical results become unreliable. There is a way to test the accuracy of numerical results without knowing the exact solution. Suppose the numerical method is of p-th order, we expect that

$$y_n^h - y(nh) = \mathcal{O}(h)^p. \tag{110}$$

This implies that

$$y_n^h - y_{2n}^{h/2} = \mathcal{O}(1 - (1/2)^p)(h)^p, \tag{111}$$

$$y_{2n}^{h/2} - y_{4n}^{h/4} = \mathcal{O}(1 - (1/2)^p)(h/2)^p. \tag{112}$$

Thus the order p can be estimated by using the formula

$$p \approx \log_2 \left| \frac{y_n^h - y_{2n}^{h/2}}{y_{2n}^{h/2} - y_{4n}^{h/4}} \right|. \tag{113}$$

We choose the initial condition $f(\omega, 0) = \frac{1}{\omega} - 0.1\omega^2$ and compute solutions for step size 0.001, 0.0005, and 0.00025 with $N = 64$. In Fig. 18, we can see that the order stays close to 4 up to the time equals to 2.5, 0.7, 1.25, and 0.9 for (a) $\epsilon = 0$ (b) $\epsilon = 0.01$ (c) $\epsilon = 0.1$ and (d) $\epsilon = 1$ respectively. Another way to test the accuracy is to check whether the area conservation holds or breaks down. The area enclosed by the interface should remain constant and it can be estimated by

$$A = -\sum_{k=-1}^{N} k a_k(t)^2. \tag{114}$$

In Fig. 19, the area A as a function of time is shown for step size 0.00025. It can be seen that area conservation (Fig. 19) and order of accuracy (Fig. 18) break down at similar time for (a) $\epsilon = 0$, (b) $\epsilon = 0.01$, and (c) $\epsilon = 0.1$. Notice that in an accuracy test the order drops to first order at $t \approx 1$ and the area conservation still holds up to $t \approx 1.3$. Similar behavior is observed for other initial conditions and different Fourier modes N. For the computational results shown in the manuscript, we show the solutions up to the time that accuracy of the solutions can be assured.

References

[1] P.G. Saffman, G.I. Taylor, The penetration of a fluid in a porous medium of Hele–Shaw cell containing a move viscous fluid, Proc. R. Soc. A 245 (1958) 312.
[2] D. Bensimon, L.P. Kadanoff, S. Liang, B.I. Shraiman, C. Tang, Viscous flows in two dimensions, Rev. Modern Phys. 58 (1986) 977.

[3] G.M. Homsy, Viscous fingering in dynamics of curved fronts and pattern selection, J. Phys. Paris 48 (1987) 2081.
[4] D. Bensimon, P. Pelce, B.I. Shraiman, Dynamics of curved fronts and pattern selection, J. Phys. Paris 48 (1987) 2081.
[5] S. Tanveer, Surprises in viscous fingering, J. Fluid Mech. 409 (2000) 273.
[6] M. Ben-Amar, Y. Pomeau, Theory of dendritic growth in a weakly undercooled melt, Europhys. Lett. 2 (1986) 307.
[7] P. Pelcé, Dynamics of Curved Fronts, Academic, Boston, 1988.
[8] D. Kessler, J. Koplik, H. Levine, Pattern selection in fingered growth phenomena, Adv. Phys. 37 (1988) 255.
[9] M. Mahadevan, R.M. Bradley, Stability of a circular void in a passivated, current-carrying metal film, J. Appl. Phys. 79 (1996) 6840.
[10] M. Ben-Amar, Void electromigration as a moving free-boundary value problem, Physica D 134 (1999) 275.
[11] L.J. Cummings, G. Richardson, M. Ben-Amar, Models of void electro-migration, European J. Appl. Math. 12 (2001) 97.
[12] U. Ebert, W. van Saarloos, C. Caroli, Streamer propagation as a pattern formation problem: planar fronts, Phys. Rev. Lett. 77 (1996) 4178.
[13] M. Arrayás, U. Ebert, W. Hundsdorfer, Spontaneous branching of anode-directed streamers between planar electrodes, Phys. Rev. Lett. 88 (2002) 174502.
[14] U. Ebert, C. Montijn, T.M.P. Briels, W. Hundsdorfer, B. Meulenbroek, A. Rocco, E.M. van Veldhuizen, The multiscale nature of streamers, Plasma Sources Sci. Technol. 15 (2006) S118.
[15] F. Brau, A. Luque, B. Meulenbroek, U. Ebert, L. Schäfer, Construction and test of a moving boundary model for negative streamer discharges, Phys. Rev. E 77 (2008) 026219.
[16] B. Meulenbroek, A. Rocco, U. Ebert, Streamer branching rationalized by conformal mapping techniques, Phys. Rev. E 69 (2004) 067402.
[17] B. Meulenbroek, U. Ebert, L. Schäfer, Regularization of moving boundaries in a Laplacian field by a mixed Dirichlet–Neumann boundary condition: exact results, Phys. Rev. Lett. 95 (2005) 195004.
[18] U. Ebert, B. Meulenbroek, L. Schäfer, Convective stabilization of a Laplacian moving boundary problem with kinetic undercooling, SIAM J. Appl. Math. 68 (2007) 292.
[19] S. Tanveer, L. Schäfer, F. Brau, U. Ebert, A moving boundary problem motivated by electric breakdown: I. Spectrum of linear perturbations, Physica D 238 (2009) 888–901.
[20] S.D. Howison, Cusp development in Hele–Shaw flow with a free surface, SIAM J. Appl. Math. 46 (1986) 20.
[21] A.S. Fokas, S. Tanveer, A Hele–Shaw problem and the second painleve transcendent, Math. Proc. Cambridge Philos. Soc. 124 (1998) 169.
[22] S. Tanveer, P.G. Saffman, The effect of nonzero viscosity ratio on the stability of fingers and bubbles in a Hele–Shaw cell, Phys. Fluids 31 (1988) 3188.
[23] J. Ye, S. Tanveer, Global solutions for two-phase Hele–Shaw bubble for a near-circular initial shape (submitted for publication).
[24] J. Ye, S. Tanveer, Global solutions for a translating near-circular Hele–Shaw bubble (submitted for publication).
[25] M. Reissig, S.V. Rogosin, F. Hübner, Analytical and numerical treatment of a complex model for Hele–Shaw moving boundary value problems with kinetic undercooling regularization, European J. Appl. Math. 10 (1999) 561.
[26] E.D. Lozansky, O.B. Firsov, Theory of the initial stage of streamer propagation, J. Phys. D: Appl. Phys. 6 (1973) 976.
[27] J.J. Sämmer, Die Feldverzerrung einer ebenen Funkenstrecke …(in English: The field distortion in a planar spark gap when it is crossed at constant voltage by an ionizing electron layer), Z. Phys. 81 (1933) 440.
[28] M. Arrayás, U. Ebert, Stability of negative ionization fronts: regularization by electric screening? Phys. Rev. E 69 (2004) 036214.
[29] G. Derks, U. Ebert, B. Meulenbroek, Laplacian instability of planar streamer ionization fronts—an example of pulled front analysis, J. Nonlinear Sci. 18 (2008) 551.
[30] A. Luque, F. Brau, U. Ebert, Saffman–Taylor streamers: mutual finger interaction in spark formation, Phys. Rev. E 78 (2008) 016206.
[31] A. Luque, V. Ratushnaya, U. Ebert, Positive and negative streamers in ambient air: modeling evolution and velocities, J. Phys. D: Appl. Phys. 41 (2008) 234005.
[32] A.J. DeGregoria, L.W. Schwartz, A boundary integral method for two-phase displacement in Hele–Shaw cells, J. Fluid Mech. 164 (1986) 164.
[33] S.D. Howison, Complex variable methods in Hele–Shaw moving boundary problems, European J. Appl. Math. 3 (1992) 209.
[34] Q. Nie, S. Tanveer, The stability of a two-dimensional rising bubble, Phys. Fluids 7 (1995) 1292.
[35] A. Iserles, A First Course in the Numerical Analysis of Differential Equations, Cambridge University Press, Cambridge, 1996.